

Medical Image Diagnostics Based on Computer-Aided Flow Analysis Using Magnetic Resonance Images

Kelvin K.L. Wong^{1,2}, Zhonghua Sun³, Stephen G. Worthley⁴, Jagannath Mazumdar², and Derek Abbott².

¹School of Aerospace, Mechanical & Manufacturing Engineering and Health Innovations Research Institute (HIRi), RMIT University, Bundoora, Victoria 3083, Australia;

²Discipline of Medical Imaging, Department of Imaging and Applied Physics, Curtin University, Western Australia, 6845, Australia;

³Centre for Biomedical Engineering (CBME) and School of Electrical & Electronic Engineering, University of Adelaide, South Australia 5005, Australia;

⁴School of Medicine, University of Adelaide, and Department of Cardiology, Royal Adelaide Hospital, South Australia 5005, Australia.

Abstract

Most of the cardiac abnormalities have an implication on hemodynamics and affect cardiovascular health. Diagnostic imaging modalities such as computed tomography and magnetic resonance imaging provide excellent anatomical information on myocardial structures, but fail to show the cardiac flow and detect heart defects *in-vivo* condition. The computerised technique for fluid motion estimation by pixel intensity tracking based on magnetic resonance signals represents a promising technique for functional assessment of cardiovascular disease, as can provide functional information of the heart in addition to analysis of its anatomy. Cardiac flow characteristics can be measured in both normal controls and patients with cardiac abnormalities such as atrial septal defect, thus, enabling identification of the underlying causes of these flow phenomena. This review paper focuses on an overview of a flow analysis scheme based on computer-aided evaluation of magnetic resonance intensity images, in comparison with other commonly used medical imaging modalities. Details of the proposed technique are provided with validations being conducted at selected abnormal cardiovascular patients. It is expected that this new technique can potentially extend applications for characterising cardiovascular defects and their hemodynamic behaviour.

Keywords: Cardiac magnetic resonance imaging; Intensity images; Fluid motion estimation; Nuclear signals; Computer algorithm; Cardiac flow analysis.

1 Introduction

Medical image techniques have undergone rapid developments over the last decade, with high spatial and temporal resolution being achieved with recent imaging modalities, such as computed tomography (CT) and magnetic resonance imaging (MRI). Thus, accurate diagnosis of cardiovascular disease can be achieved with these techniques. In addition to the diagnosis of cardiovascular disease based on anatomical changes, these modalities allow for assessment of cardiovascular flow, and thus providing a new paradigm shift in the diagnostic management of cardiac diseases. Potentially, flow information can be utilised for cardiac health grading [1-5]. Therefore, cardiovascular flow quantification via *in-vivo* MRI [6-8] is a significant motivation for the development of health diagnostic systems from a clinical perspective. Quantification of vortices in heart chambers [9, 10] has potential utility for clinical study of cardiac disease even in the absence of the well-established phase contrast velocity-encoded magnetic resonance imaging. The concept may be extended to study atrial septal defects pre- and post- surgical treatment. Flow characterisation based on vortical flow analysis [11] promises high quality research and has significant clinical value. Since no fluid mechanical flow quantification has been systematically investigated from cardiovascular flow, for diagnosis of the cardiac disease, a technique of cardiac flow analysis via medical imaging provides an alternative approach for characterising cardiac abnormalities.

Current state-of-the-art flow evaluation techniques are related to transthoracic and transesophageal echocardiographic systems [12-19]. The use of ultrasound devices has been well-established in assessing cardiovascular flow and is a predecessor to MRI technology. However, with the rapid advancements in MRI, and increased production based on a larger economy of scale have all contributed to the lowering of the cost of such imaging systems, thus leading to the increase of their use for cardiac flow assessment. Cardiac MRI has been advanced to a stage with high spatial and temporal resolutions satisfactorily achieved. While the main shortcomings are lack of wide availability of MRI scanners and long duration of scanning, higher quality images, along with embedded functional information for cardiac structural and flow assessment compensate for these limitations. .

Cardiac diseases remain a major cause of mortality in advanced countries. Due to the aging population and epidemic situation of obesity, the increase in incidence of heart diseases motivates the need for therapeutic devices dedicated to the effective treatment of cardiovascular diseases.

The shift in MRI technology for cardiac diagnosis is reported to be functional imaging that pertains to the fluid dynamics of blood in the heart. As such, there will be an increasing demand for cardiac flow analysis technique to facilitate the diagnosis and prognosis.. Using MRI, computer-aided fluid motion tracking of the image intensities can prepare the flow assessment reports for clinical studies in the event of the absence of a dedicated blood flow velocity measurement protocol. It utilises the dynamic representation of magnetic resonance signals to predict the bio-fluid motion.

The preliminary studies conducted have reliably demonstrated that flow characteristics differ in patients with cardiovascular defects pre- and post- surgical correction. In this aspect, the proposed method of a computerised magnetic resonance fluid motion tracking is promising in its clinical utility. Future research will look at combining myocardial structural and flow information from various medical imaging devices or therapies, and build a more concise report on cardiac abnormalities.

1.1 Scope of Review

This paper reviews the fundamental theory underlying nuclear magnetic resonance; from the examination of hydrogen proton spins, through to the development of MRI machines that are able to provide two-dimensional images of the human body at any angle and orientation. It also describes applications related to imaging of the heart, as well as laying the groundwork for examination of cardiac anomalies and diagnosis of heart diseases using MRI.

We examine the mechanics of MRI and document the definitions of terminologies and underlying related theories. The motivation behind this paper is to enable the understanding of outputs delivered by this imaging modality. Cardiac imaging and flow tracking using motion estimation are the key focus of the research undertaken, and the critical issue is to understand the type and nature of signal features to track. Therefore, the theoretical discussion ranges from explaining the effects of the magnetic field on hydrogen nuclei, to the alignment of spins on registration of nuclear signals of a living body during MRI scanning [20, 21].

The physics and engineering of MRI for the detection and analysis of heart defects in patients are presented. This medical imaging modality can provide superior tissue-blood intensity contrast in output images, which can be used to identify the abnormalities in the myocardium. Because of the incoherent proton-spin alignments in high-speed turbulent cardiac flow, the temporal blood signals can be traced visually to analyse abnormal flow patterns. In this paper, we outline the guidelines for examining patients diagnosed with an atrial septal defect. The aim is to provide a series of reliable procedures and concepts to be effectively deployed for diagnosis of such cardiac defects. Automated vortex tracking may be achieved by the use of motion

tracking algorithms. Such a systematic approach can be implemented in hospitals to support indication of the degree of abnormality and to provide expert opinion to the patient.

We examine some of the well-established particle image velocimetry (PIV) systems that are used to generate accurate time-resolved vector fields of up to three spatial dimensions. It is interesting to highlight that such flow tracking can be classified as optical-, magnetic resonance- and ultrasonic- image velocimetry. In our context, the MR-based PIV does not refer to the well-established velocity-encoded phase contrast MRI, but the MR-based tracking pertains to fluid motion tracking [9, 10]. We are interested to examine in-plane flow field generation using the different types of imaging systems for PIV.

The choices of a computer-assisted fluid motion tracking include magnetic resonance- and ultrasonic- image velocimetry. For the latter technique, contrast-enhanced echocardiography with PIV application, which is also known as echo-PIV, may be achieved by the use of an intravenous contrast agent [22, 23]. However, the method is limited to the availability of such echo-enhancing agents. By contrast, MR-based tracking makes use of asynchronous proton spins as optical markers and eliminates the use of contrast agents [9]. This highlights the superiority of MRI over contrast-enhanced echocardiography with fluid motion tracking. Considering the wide range of topics in reviewing all three types of imaging and velocity tracking systems, we will limit the scope of review to only MR-based PIV, also known as MR fluid motion tracking.

2 Theory of Nuclear MRI

2.1 Utilisation of Magnetic Resonance

We examine nuclear magnetic resonance (NMR) imaging at a basic level to elucidate the quantum mechanical concepts. When an organic structure is positioned within the centre of an external magnetic field it becomes itself partially magnetised with a magnitude of comparatively lower order. The assemblage of hydrogen nuclei (protons) in the water molecules within the body will be perturbed with radio frequency radiation. The nuclear spins then realign with the magnetic field and emit radio frequency (RF) waves during this longitudinal relaxation period [24]. The duration of the nuclei realignment and emission of RF signals can then be represented by MR images that we use for examination. Since the emission rate of RF waves is dependent on the type of material that contains the nuclei, different intensities of pixels can distinguish various anatomical structures. As such, MRI is the application of magnetic fields and usage of radio frequency pulses to image different tissues in the human body [12, 13, 25, 72]. The magnetic resonance registration is based on the response of specific nuclei to the exposed radio frequency energy and can be represented using an intensity-based image [73, 74]. The emitted signal can be

encoded in such a way that the induced time-varying voltage in a receiver coil surrounding the object or patient, which correspond to the spatial position of signal from the excitation of spin $\frac{1}{2}$ protons, are used for construction of an image slice. An MRI scanner is effectively a device that creates a map of spin relaxation times of hydrogen nuclei within the tissue. This allows the structures to be scanned at a planar section [24]. MRI also allows multiple contiguous slices at various sections of the body to be scanned at various phases of one cardiac cycle. Therefore, cine-MRI can be presented at various phases continuously for motion analysis of cardiac structures.

Two major imaging sequences or techniques used in MRI are spin echo and gradient echo, which are based on the principle of magnetic resonance described in previous sections. Other types of imaging have been developed in the past decade. Thus, we shall briefly review some of these imaging sequences.

Spin echo imaging provides good tissue discrimination of the cardiac structures in heart with flexible contrast characteristics depending on the programmed parameters of imaging sequence. These may include T_1 weighted (T1W), proton density weighted (PDW) and T_2 weighted (T2W) imaging. The spin echo imaging technique is also called *dark blood imaging* as blood within cardiovascular compartments appears black.

Gradient echo imaging is especially useful for assessment of myocardial function and may be acquired rapidly, allowing cine imaging of the heart. It is commonly known as *bright blood imaging* as the imaged blood appears white [25, 26]. However, gradient echo imaging provides poor tissue contrast as compared to the spin echo based technique. Therefore, there is a need for a fast-imaging sequence that allows for scanning with a better contrast between blood and myocardium.

Steady-state free precession (SSFP) is a method of MR excitation [27-29], which uses steady states of magnetisation and hence given its name. SSFP is an enhancement of the gradient echo sequence in which a non-zero steady state develops for both components of magnetisation (transverse and longitudinal) and also when RF pulses are rapidly applied repeatedly with inter-pulse intervals that are short compared to both T_1 and T_2 of the tissue. If the RF pulses are close enough together, the MR signal will never decay completely, so that the spins in the transverse plane will also not de-phase completely. Due to its superiority over gradient echo imaging, SSFP sequences are now commonly used in MRI.

Subsequently, a variation of SSFP gives rise to the balanced SSFP (b-SSFP) [30, 31]. This protocol is capable of imaging cross-sections of cardiac structures with unsurpassed soft tissue contrast [25]. It is one of the most popular medical imaging modalities for the registration of physiological properties of the heart and arteries. The b-SSFP sequence combines both

longitudinal and transverse magnetisation [32]. Based on complex T_1/T_2 -contrast configurations [33], such imaging sequence refocuses all gradients over a repetition interval to achieve fast-imaging with a high signal [32]. With the rapid development of MRI technology, steady-state free precession MRI protocol is demonstrated in the literature as providing high quality scans for cine cardiac MRI [34-36] and is commonly used today.

2.2 Asynchronous Proton Precession

The precessing coherence of nuclear spins is related to the motion state of the fluid, which contains the nuclei, and can give signal contrast that corresponds to its flow. This is the first description explaining the dynamic magnetic resonance signal contrast that relates to the motion of blood in the heart chamber. We harness the phenomenon and built a technology based on this concept to track blood flow. We examine the theory governing the concept of void signal registration due to turbulence within a fluid, where atomic nuclei have been aligned either parallel or anti-parallel to a powerful and uniform magnetic field. As high energy nuclei relax and realign, they emit energy with certain properties that are recorded to provide information about the medium. Image contrast is created by weighting the energy signal during realignment of the nuclear spins with the magnetic field. A signal image is then generated as a result of this quantum mechanical activity.

As the fluid is transported, the nuclear signal within the fluid follows its displacement. In a turbulent flow, the diffusion of magnetic moments or proton spins occurs [37]; however, the Reynolds number of cardiovascular flow is typically too low to have an effect on signal de-phasing that arises from the diffusion of spins. However, de-phasing by asynchronous precession of spin due to turbulence in the flow (Figure 1) can reduce MR signal during imaging [38, 39]. Low MR signals are represented as higher pixel intensities in the MR image. The proton spins de-phase in the transverse plane when the RF pulse is terminated. Other than the cause of uncontrolled alignment of magnetic moments in turbulent fluid, this de-phasing can also be due to intrinsic non-homogeneities of the magnetic field as a result of magnetic susceptibility changes at tissue interfaces.

Therefore, there is a reduction in the signal registration on the image. Asynchronous proton spins at this point are represented by a reduction in signal intensity registered onto the image [38, 39]. As the variation of nuclear spin alignment follows the movement of the fluid in a channel, there exists a change of signal intensity in the direction of flow. This produces a pattern of varying intensity in the magnetic resonance image. The movement of this pattern is called intensity flow. The presence of the temporal intensities, represented by pixels of the image, coincides with the blood flow, and can be visually observed from time-dependent sequences of magnetic resonance images. Motion estimation [40] via the image processing of MR images can

provide a more automated technique of analysing the flow; however, it requires the engineering of a multi-resolution optical flow platform to achieve this [41].

2.3 Application of MRI in Cardiac Diagnosis

It is a well-established fact that cardiac MRI possesses superior resolution, good blood and tissue contrast and offers a wide topological field of view. Unlike X-ray based techniques, it is a non-ionising modality. The special properties of MRI allow physicians to examine abnormal cardiac morphology as a means of predicting possible heart diseases. Besides morphological imaging, cardiac MRI also allows myocardial wall tracking [42, 43], calculation of ventricular and stroke volumes, mass, ejection fraction [6, 38], and demonstration of myocardial perfusion in ischemic heart diseases [44, 45].

Cardiac MRI allows multiple contiguous slices at various orientations to be scanned at various phases of one cardiac cycle. Typically, the scan pertaining to cardiac analysis can either be short axis (SA) or long axis (LA) as shown in Figure 2, and based on the two-chamber (2C), three-chamber (3C) or four-chamber (4C) configurations as illustrated by Figure 3.

Cardiac MRI has been widely investigated for imaging patients with aortic diseases such as aortic dissection [46-48], aortic aneurysm [49, 50], atherosclerotic coronary artery, as well as human hearts with myocardial wall diseases such as atrial and ventricular septal defect [51-54]. However, traditionally, only anatomical information of the cardiovascular compartments or structures was used for diagnosis, until the development of phase contrast MRI cardiac flow quantification can be achieved.

For monitoring atherosclerotic arteries, steady-state free precession magnetic resonance angiography (MRA) has the advantages of obtaining high signal imaging of coronary arteries without contrast agents [55]. Therefore, coronary artery imaging with MRA is typically performed to extract information on arteries and stenoses. However, such imaging is restricted to arterial wall information and relates only to visualisation of the arteries. In relation to flow measurement within such micro-structures, magnetic resonance image velocimetry is able to reveal coronary artery luminal narrowing [56-58]. However this is limited to the availability of a velocity measurement protocol and dedicated phase contrast magnetic resonance protocol is usually only available in high-end MRI machines. The implementation of MRI is only applicable to examining coronary arteries if the resolution of the MR images is sufficient to capture velocity-encoded blood signals sufficiently. The improvement of cardiac MRI in terms of resolution will help to increase the accuracy of flow tracking since more signal features can be encoded within the images. Therefore, an important criterion is the required increment in pixel resolution of MRI for micro-scale arteries. However, this will come at the expense of computational cost, and lead to increased processing time. High performance imaging with

superior resolution MRA for delineation of vascular disease may be achievable with 3.0 Tesla MRI.

We summarise the clinical applications of MRI in the cardiovascular system for which medical conditions (pericardial disease, congenital heart disease, aortic arch heart disease, acquired heart disease, cardiac transplantation, atrial and ventricular septal defects, atrial fibrillation, valve regurgitation, aneurysms, coarctation of the aorta, and atherosclerosis) may be assessed [59].

We limit the scope of our review by emphasising the use of cardiac MRI for the investigation of atrial septal defect (ASD) with quantitative assessment from the perspective of cardiac chamber flow, and illustration and data supporting the analysis of this cardiovascular problem is provided as an exemplification of the clinical utility of cardiac MRI.

3 Theory of MR Fluid Motion Tracking

3.1 Computer-Aided Visual Motion Tracking Using Cardiac MRI

For estimation of non-rigid motion such as MR-signal features, we expect to see a wide variation in signal flow behaviour ranging from elastic deformation and segregation to non-uniform volume changes. Motion perception by humans is a natural, well-evolved capability with the facility to rapidly categorise relative motion among fluid structures with respect to multiple coordinate systems. The challenge, therefore, is to develop a fluid motion tracking system that can automatically detect such complex flow.

We have provided a framework that enables the development of MR fluid motion tracking such that a successful application of this technique may be able to perform computational flow prediction of blood motion based on nuclear signals measured using MRI [9, 10], and devised an effective platform for visualization of the flow [60]. Estimating motion by harnessing image signals of varying spatio-temporal intensity can be achieved. This theory is based on observations which we can deduce with our intuitive understanding of visual motion registration. In the context of electromagnetic signals which is analogous to magnetic resonance signals, and based on our knowledge of identifying motion by referencing contrasting moving light sources, we state Observations 1 and 2 as follows:

Observation 1: *The movement of light lines can be perceived as the movement of shadow lines on the illuminated background. In our world of vision, light and darkness are the signals of opposite magnitudes that are used in determining motion.*

Observation 2: *When observing blood movement in magnetic resonance images of the heart, it is a mixture of observing moving dark shadows of asynchronous proton spins among the bright imaged blood, and moving bright shadows of synchronous spins among the contrasting imaged blood.*

The computerised motion tracking technique makes use of the moving accumulation of asynchronous spin phase shifts. The incoherent spins cause the blood to appear dark in SSFP MRI. Apart from passing blood through heterogeneous magnetic fields, turbulence in blood flow as well as blood from other regions of flow entering into the scanned slice may consist of different spin shifts from the imaged region of interest. It is the in-plane tracking of such asynchronous spins that allows the velocity field of blood to be developed. We can safely conclude that since the dark regions represented by these irregular spins correspond to the general flow path of the blood, the perception of motion developed from their intensity shifts may very well be correlated to the actual cardiac flow speed and direction as shown in Figure 4.

If the blood containing a collection of spins (X) that has coherent phases leaves the slice of interest perpendicularly, and a new region of blood with incoherent spins (Y) with multiple degrees of phase shift enters the same slice at the same point, the pixels region at that point turns from white to black. Therefore, the motion estimation algorithm identifies the blood in that region as stationary in-plane, which is true. Note that there is in fact no specific motion in-plane but a velocity component through-plane.

Our aim is to track flow patterns, that pertains to the in-plane orientation. Note that we are not registering the spin phase difference and extracting the velocity information from it. The tracking is of a different nature in that we estimate the pixel displacement presented by the movements of a collective group X within a region filled with Y or vice versa.

Let us assume that we have a collective group of spins Y moving in the in-plane direction. This appears in the image as a dark stream of moving pixels across the region. This time, the algorithm is able to track the movement in the plane using the pre- and post- sequence of cine-MR images. The flow 'tracking' fails only when we have a group of X and no Y group spins that are imaged. The movement of white pixels against a white background cannot be picked up. However, this will never occur in a cardiac chamber as the flow within definitely comprises of a variety of different spins phases.

Traditionally, the visual deduction of blood movement using SSFP MRI has been carried out by doctors to examine ASD patients. The explanation of the quantum mechanical effects governing this phenomenon is not well documented in current literature, and moreover, there is a lack of proper procedure to use such information for clinical diagnosis, this method is generally quite effective and conveniently used by medical doctors to understand the difference in flow

behaviour in a cardiac chamber. The flow patterns can be traced by simple observation with cine-MR images being played back at an appropriate speed to register the motion into the human brain. However, a reliable computerised system for visual tracking can be developed for the image analysis, especially when the images are displayed at rates higher than human-assisted visual review processes. These two observations form the fundamentals for developing the computational motion estimation that are outlined in this study and ultimately leads us to the application of tracking magnetic resonating blood to develop cardiac flow velocity fields [9, 10].

The system integration of the medical imaging and computational processing components gives rise to a diagnostic system that can be used for assessing the cardiac condition of patients with cardiovascular disease (Figure 5). This constructs a system for analysing cardiac defects via examination of the flow variations derived from MRI and post-processing techniques.

MRI can be used to provide a set of standard results for evaluating abnormal cardiac behavior and provide a basis of analysis. Imaging planar sections of the heart through the cardiac chamber is one of the pre-requisite selection criteria for tracking vortical blood flow, since a vortex can be best characterised if a sectional slice is taken orthogonal to the axis of rotation and presented in the plan view. Cardiac MRI or scanning protocols allow imaging to be registered within the body at localised sections with specific depth and thickness (Figure 6).

3.2 Validation of MR Fluid Motion Tracking by Intensity Images

A number of effects related to complex turbulent flow and intra-voxel dephasing, as well as view-to-view phase changes can influence signal intensity. In addition, local changes in the magnetic field can influence signal intensity may be falsely interpreted as flow related signal changes. MRI using SSFP relates to complex signal behaviour, which is related not only to flow but also strongly depends on local magnetic field inhomogeneities. From the fluid dynamics perspective, highly asymmetric flow causes the signal loss as a result of the rapid influx of proton spins into a volume of interest and intra-voxel dephasing during the registration time gap when asynchronous alignment of the spins takes place. Clinical observation of blood flow is required to examine this type of natural phenomenon from intensity motion of cine magnetic resonance images that pertain to the heart chamber. Verification of the multi-resolution fluid motion tracking requires a controlled comparison of a known intensity flow with the tracking results. And finally, the validation of the technique may be performed *in-vivo* by experimental phase contrast velocity MRI. In general, our validation comes in three parts: *Computational*, *Experimental*, and *Clinical validations*. The key descriptions of these validations are as follows:

Computational validation- MR fluid motion tracking can be computationally verified based on ground truth data that is synthetically produced [10]. This gives rise to tracking artificially generated intensity grids that are circumferentially oriented about the centre of rotation. Tracking

of the rotating intensity grids, utilization of a pyramidal optical flow technique and comparing the computed circumferential and tangential velocities with flow fields from an analytical Lamb-Oseen vortex, forms the basis of our computational verification.

Experimental validation- The *in-vivo* phase contrast MRI experiments have been performed to compare against MR fluid motion tracking with good agreement [9]. However, it is more appropriate to experimentally test the technique onto a healthy and strong case subject since long breath holds are required to ensure quality imaging. Note that fluid motion tracking errors that may arise due to poor imaging or signal quality are usually averaged out in the algorithmic implementation and during vorticity mapping. It may be worthwhile emphasising that slight deviations in accuracy of tracking do not raise significant concerns during the analysis of the vortices in cardiac chambers since errors are usually reduced during numerical formulation of vorticity, which involves averaging of velocity vectors [11].

Clinical Utility - Demonstration of the clinical utility by applying MRI onto ASD is a long process, which requires validation by other imaging modalities. Very often, it is difficult for clinical centres to approve such an extensive phase contrast MRI imaging procedure for investigation of the ASD patient due to health and safety reasons even though a velocity-encoded imaging protocol is present. For phase contrast MRI, the chances of obtaining a sufficiently good resolution and quality velocity-encoding scan for a cardiac patient will be low since respiratory breath hold (that is required to avoid ghosting artifacts during MRI) is a major issue for an ASD patient. For echocardiography or Doppler ultrasound imaging, the velocity flow measurements are taken along the direction of the ultrasonic beam, and therefore, this modality requires geometrical transformation when resolving vortical flow within a cardiac chamber in planar scans. As our analysis in this review is based on the characterisation of atrial vortices, the best tool for evaluating rotational flow in a plane for ASD patients is suggested to be magnetic resonance fluid motion tracking.

3.3 Other Considerations of Computer-Aided Fluid Motion Tracking Based on Intensity Images

It may be useful to implement motion estimation algorithms [40, 41] for tracking of volatile fluid imaging. This may then help in enhancing the flow field tracking accuracy. Investigating the tracking of deformable objects [61-63] can give us a further insight into improving fluid motion tracking, and the studies have shown that it is possible to obtain a meaningful optical flow of deformable liquids and gases. These techniques developed in computer vision may be worthwhile investigating and employing these algorithms as an alternative to multi-resolution Lucas Kanade optical flow used in the MR fluid motion tracking system may be carried out.

Extension of MRI to the study of flow phenomenon is not new and can be applied to solve problems directly relevant to multi-phase flow visualisation and analysis [64-68]. The state-of-the-art studies in MR flow imaging are previously discussed and the framework can be applied to

investigate cardiac blood motion as well. Emerging technologies, such as MR global coherent free precession (GCFP) [69, 70], provide a new platform for the application of MR fluid motion tracking, which generates a potential scheme for cardiac flow tracking. Such MRI protocols can be applied to blood spin labelling techniques for acquisition of multiple temporal slices of gray-scale intensity blood flow or cine-angiograms without a contrast agent and use of ionising radiation [71]. The movement of blood can be tracked as a result of processing such information using fluid motion estimation. Sample GCFP images provide information about vascular function and morphology just as SSFP MRI does. Moreover, it provides us with a more definite contrast of spin labelled dynamic blood into the non-spin labelled region because of the tagging of blood protons every few milliseconds as they travel through an arbitrary region in space. At higher magnetic field strength, such as 3.0 Tesla in clinical settings, the registration of intensity blood motion is performed at resolutions (higher than those of 1.5 Tesla) to image higher resolution anatomic and physiologic details, and also providing higher quality images to facilitate a computer-aided fluid motion tracking. However, it is worthwhile noting that significant dynamic intensity contrast of the motional blood in cine mode is required for the motion tracking algorithm to function properly.

4 Diagnosis of Cardiac Defect by Medical Imaging

4.1 Diagnosis by MR Fluid Motion Tracking—An Extension of MRI Processing

There have seen a plethora of significant advances over the last decades in MRI with relevant applications in medical imaging of the heart. However, there has been a lack of proper qualitative explanation of some observed phenomena such as gray-scale intensity variation of the imaged cardiac blood. Therefore, this review sets the scene for the further development of MR fluid motion estimation by providing the theoretical explanation for signals of contrasting intensity due to asynchronous proton spins in dynamic fluid and how they arise. Various MRI protocols, concepts and terminologies are covered in appropriately organized sections.

Cardiac MRI can be used to reveal their health status. Cardiac defects such as atrial septal defect (ASD) exist in approximately 0.5% of heart disease patients. ASD can be detected by physical examination and imaging modalities including chest radiography, echocardiography, cardiac CT or MRI scans [53]. Functional medical imaging is able to provide an alternative method for measurement and quantification of the blood flow rotation (defined as vorticity) in the heart of patients diagnosed with ASD. The superiority of cardiac MRI over chest radiography and CT is the absence of radiation exposure and that the imaging modality allows follow-up exams, especially in children. In most cases, once ASD is confirmed, the accepted surgical treatment is septal occlusion [75].

In addition to conventional MRI techniques, it may be of interest to examine the flow information pertaining to cardiovascular structures parallel to viewing the myocardial defect. For example, using measured data such as phase contrast magnetic resonance images, we can also develop a procedure for evaluating dynamic flow changes within the heart chambers; in particular, the quantification of the (1) variation of blood velocity with respect to time, (2) cross-sectional blood flow profile, and (3) rotational characteristics (vorticity) of flow in chamber. The rate of blood rotation is related to pressure within the heart chamber, and can be used to assess the degree of septal defect before and after septal occluder insertion. Such a method is particularly useful for evaluating the risk inflicted on patients diagnosed with such cardiovascular diseases before and after surgical intervention, and therefore offers great clinical benefit to medical doctors when used in conjunction with the examination of the physical septal defect. However, velocity-encoded scanning such as the phase contrast MRI is time consuming and requires the use of special software for flow visualisation. Therefore, we propose an alternative method for assessing flow qualitatively based on a steady-state free precession MRI protocol.

4.2 Alternative Imaging Techniques for Diagnosis

In general, the use of cardiac MRI for heart diagnosis is effective and accurate. Despite the high resolution in the imaging of cardiac tissues and blood, this imaging modality is limited by longer duration scan and is generally expensive. Although the cost of the examination is high, its price reduction will be contributed by scale of manufacturing and improvement in the technology in the near future. The use of other existing medical imaging modalities can also enable visualisation of the intrinsic structure of the heart and/or determine flow properties within the heart chambers and arteries. We will now review and compare other imaging methods that can be used to diagnose cardiac abnormalities. The technical details of echocardiography, chest radiography and computed tomography, as well as their implications in the diagnosis of ASD will be described here. In addition, one may refer to Table 1 for an overview of the advantages and disadvantages of these techniques.

4.2.1 Echocardiography

The echocardiogram is an ultrasound scan of the heart that may be used for assessing ASD patients [53, 76, 77]. Using standard ultrasound scans, two-dimensional views of the heart can be obtained and used for flow visualization. In addition to creating scans of the cardiovascular system, the echocardiogram can also assess the velocity of blood and cardiac tissue at any arbitrary point using pulsed or continuous wave Doppler ultrasound [78-80]. This allows functional assessment of cardiac disease such as abnormal communications between the left and right side of the heart, as well as any shunting of blood through an ASD.

Ultrasound is able to detect blood flow, which makes it potentially applicable to study flow visualization. However, this technique is most commonly used as a qualitative technique and is liable to error depending on the plane of imaging and operator experience. Contrast agents, such as a suspension of microscopic gas bubbles, are used to enhance ultrasound performance. Ultrasound is, however, widely available and an inexpensive alternative to MRI and CT methods, and therefore more commonly used to diagnose ASD.

Ultrasound is a radiation free modality, and thus avoids the harmful effect to the body due to x-ray radiation. But its performance is often limited by the availability of a clear acoustic window between the external surface and imaged region. Moreover, it is difficult for ultrasound imaging to be performed on a cross-sectional plane of the chamber. Ultrasound scans typically measure channel flow in the blood vessels and not planar flow through the heart chamber. As a result of this limitation, it is difficult for us to investigate the vortices in the blood within the heart chamber using ultrasound.

Although transthoracic and transesophageal echocardiography are now regarded as the standard for ASD assessment [12-19], clinical trials will be the subject of future studies to show incremental value in using cardiac MRI flow analysis. Advancements in software support for contrast echocardiography [22, 23] can pave way for future diagnosis of cardiac defects by means of flow analysis within cardiac chambers.

4.2.2 Chest X-Ray

Radiographic techniques produce image films by registering the intensity of X-rays passing through a human body. The two-dimensional chest radiograph can be represented using an intensity image [81]. Variation in the density of tissues results in different degrees of attenuation of X-ray photons within the structure under exposure and gives the intensity contrast of tissues captured on film by casting a distinctive image of shadows on it. The use of ionising radiation may harm the body if there is excessive exposure. Due to the inability to register signals from localised regions, the scan is unable to produce an image registering a projection slice at a specific depth through the body. The conventional chest X-ray can detect and monitor cardiac disease [31]. Chest X-rays can show up abnormalities in patients with severe ASD. Right heart dilation can be observed in lateral films. The central pulmonary arteries are characteristically enlarged with pulmonary plethora indicating increased pulmonary flow, and this can be used to diagnose ASD [53, 82].

4.2.3 Computed Tomography

Computed tomography (CT) represents a technical revolution in medical imaging as it provides excellent anatomical details of the body organs [83]. Cardiac CT has become increasingly used

in clinical practice due to improved spatial and temporal resolution, with high quality images acquired using retrospective ECG-gating. High diagnostic accuracy has been achieved with cardiac CT in the diagnosis of coronary artery disease. However, CT does not provide any information on the hemodynamic significance of ASD and is associated with high radiation exposure, which results in radiation-induced magliancy. Hence, its value in the diagnosis and management of patients with ASD is limited. The CT scans are often used to check if the right heart chambers are dilated or the location and size of a septal defect, which can serve as an indication for the severity of ASD.

4.3 Diagnosis Based on MR Fluid Motion Tracking by Intensity Images

MRI that is coupled with computer-aided fluid motion tracking and cardiac flow analysis [84, 85] gives rise to a system of visualisation and analytical processes, which can describe flow behavior in cardiac chambers by processing magnetic resonance images of blood in motion. Unlike velocity encoding (VENC) imaging techniques such as phase contrast MRI, our framework [9, 10] uses standard cardiac MRI protocols.

MRI allows multiple contiguous slices at various sections of the body to be scanned at various phases of one cardiac cycle. Therefore, cine-MRI can be presented at various phases continuously for motion analysis of cardiac structures. Therefore, the assessment of ASD has been performed on cardiac MRI effectively. Examination using spin-echo cine-MRI, which gives a good intensity contrast for the cardiac wall, is able to reveal ASD [75]. In addition, gradient-echo T1-weighted cine-MRI of cardiac chambers allows visualisation of blood movement, based on the shifting intensity in the image shown up as varying degrees of signal voids due to de-phasing of nuclear spins. Apart from the left-to-right shunting of blood that can be observed, the enlargement of the right atrium can also be detected using MR images.

The use of computerised MR fluid motion tracking applied onto cardiac imaging of right atria enables a good assessment of vortices that exist in the heart (Figure 7). We understand that such flow generates vortices [86] and is essential in efficient heart operation and blood circulation [87]. The study of vortices in the human heart has been extensively performed using phase contrast data [88]. The quantification of intra-cardiac flow using a velocity field gives information on the vortical blood flow.

Technique for evaluating the nature of flow in the heart and arteries based on magnetic resonance fluid motion tracking and vorticity flow visualisation forms the current state-of-the-art technology [9]. Diagnostic systems for detecting cardiac abnormalities and quantifying the degree of defect have proven to be clinically attractive. Such information will have useful future practical benefit for the assessment of cardiac-related abnormalities.

This system is vital because of the technical feasibility of using measured information from MRI without affecting its usual scanning mode to determine blood flow information. The key success is the result of implementing MR fluid motion tracking as a post processing tool for images that are output by MR scanners. This renders the encoding of velocity information redundant which reduces scanning and processing time. MR flow image reconstruction based on fluid motion tracking opens up many new opportunities for flow analysis concurrent to the examination of cardiac chambers, septal defects, and heart valve behavior. It may also be of interest to cardiologists and physiologists for providing information on the structural change of cardiac chambers that is related to flow phenomena in the heart.

Bio-fluid motion tracking framework can present a visualisation application with unique quantification of flow behaviour that will lead to a viable diagnostic system for evaluating cardiac related failures or health risk in patients (Figure 8). The ease and speed of preparation makes it useful for medical doctors to quickly gain insights into the flow structures in the defective regions of the heart and to assist in strategising surgical procedures, operations or artificial implantations.

5 MR Technique for Cardiac Defect Examination: A Clinical Case

5.1 Examination and Surgical Intervention

The ASD is a congenital cardiac abnormality that affects the health and fitness of the individual. In this medical condition, a puncture in the septum exists to create a left-to-right shunt of atrial blood to maintain equalisation of pressure in the heart. Due to this flow phenomenon, oxygenated blood seeps through the left atrium to the right one instead of being effectively circulated to the rest of the body. As a result, the patient experiences a lower efficiency of oxygenated blood circulation. The schematic diagram in Figure 9A illustrates the inefficient replenishment of oxygenated blood and its reduced flow from the left atrium to left ventricle and ultimately through the aorta to the rest of the body. Figure 9B shows the location of the septal defect on the right atrium where the left-to-right blood shunt takes place.

Atrial septal occlusion (ASO) is the surgical correction to this cardiac situation by delivery of the right atrial occluder disc to the location of the defect using catheterisation [89-91] as demonstrated in Figure 10. It is proposed that an indication of difference in the pre- and post-surgical intervention exists. The natural flow of blood in a rotational fashion is disturbed in a cardiac chamber with a septal defect. One of the hypotheses for a less consistent blood flow rotation before the operation is the reduction in the velocity of blood circulating in a larger chamber as a result of left-to-right shunt that causes the right atrial dilation. The other reason is that the leak produces a jet of fluid through the defect to break up the vortical flow in the right

atrium into multiple vortices. Once the septal occluder is inserted to close the defect, the left and right chambers are restored to their more normal sizes, and a more consistent right atrial blood rotation may be present (Figure 10).

5.2 MRI Equipment and Imaging Parameters

5.2.1 Cardiac Chamber of Interest

It is hypothesised that the vortices, which are generated in the right and left atria pre- and post-septal occlusion, possess different strengths [9]. The right atrium is enlarged due to a left-to-right shunt and the changes in the signal intensity of blood using MRI is more easily detected than in the other chambers. We choose the right atrial flow for analysis, since this is the chamber where we can observe the shunting of blood into it from the left atrium.

MR images of the heart at short axis (two-chamber) view may be performed and used for visual flow analysis to confirm our hypothesis. We note the observation of varying degrees of signal voids within the local region with poor gradient refocusing as the result of chaotic and dynamic blood flow in more than one plane. As these local turbulent regions move along with the global flow of the blood, we will be able to visually track their magnitude and direction of movement and determine the flow structure. However, there has been no method that performs flow quantification and as such, only a qualitative examination of the flow can be performed at this stage. The assessment of ASD has been performed on cardiac MRI effectively. Examination using spin-echo cine-MRI that gives a good intensity contrast for the cardiac wall is able to reveal ASD [92]. In addition, gradient-echo T1-weighted cine-MRI of cardiac chambers allows visualization of blood movement, based on the shifting intensity in the image shown up as signal voids due to de-phasing of nuclear spins. Apart from the left-to-right shunting of blood that can be observed, the enlargement of the right atrium can also be detected using MR images.

The use of SSFP MRI can be illustrated using Figure 11. We observe the discontinuity in the septum that allows blood to shunt from the left atrium (LA) to the right atrium (RA). Moreover, in a normal right atrium, the chamber blood flows in a rotational manner. This vortical flow is disturbed by the shunting of blood to cause multiple small-scale vortices to appear. As a result, the efficiency in blood circulation is affected. In addition, we also note the difference in right atrial chamber size between the pre- and post-ASO conditions since the percutaneous closure of ASD can reduce the right heart volumes by removing the left-to-right shunting [93].

5.2.2 Experimental Procedures

The flowchart that is presented in Figure 12 provides an illustration of the procedures for the investigation of ASD. Each procedural step is described in point form and provides a guide for the radiologists and/or investigators in its execution. Flexibility in adjustments of the steps can be made or additional operations can be incorporated into this activity depending on the configuration of the machines and setup used in the facilities. The flowchart is designed to guide the medical imaging, observation of cardiac abnormalities, and deduction of flow as well as analysis of the vortical flow information for investigation of atrial vorticity in relation to septal defects. Procedures related to the flowchart are detailed as follows.

1. SSFP based on a Siemens Sonata, 1.5 Tesla, model–syngo MR 2004A scanner with Numaris–4, Series No: 21609 software is performed using contiguous slices in short axis (two-chamber) orientation through the heart. All images are acquired with retrospective gating and a typical number of 25 phases (or time frames) for each slice is obtained. Acquisition parameters may be different for scans of pre- and post- occlusion of ASD. The scanned images are loaded into Siemens syngo Multi Modality Workplace system. The Multi Modality Workplace is a stand-alone evaluation system that can be embedded in a workplace network. Note that the balanced SSFP (b-SSFP) imaging protocol is provided by the Siemens MRI scanner.
2. The cardiac abnormality is further verified by viewing the cine-MRI of the patient using media player incorporated within the system. The subjects with ASD can be identified based on morphological defects such as the discontinuity of the atrial septum and/or dilation of the right atrium. Left-to-right shunting of blood through the septal defect can be observed by assessing the cine-MRI.
3. The scanned images in DICOM format are transferable to a removable storage device (i.e. CDRs/DVD-Rs and CD/DVD drives, magneto-optical discs and drives, or diskette drives) for storage and transfer. The syngo Media Viewer, which is a DICOM viewing application, can be burned to CD or DVD so that imaging studies can be viewed on personal computers. Images may then be processed offline.
4. Patient particulars and scan records are entered into a patient database. With the labeling of scan information, future retrieval of cases pertaining to the different types of cardiac condition can be performed by labeling the cardiac condition field accordingly.
5. A new database of ASD patients is created for study.
6. Retrieval of cases pertaining to ASD is performed by referencing the database of patients who underwent scans. In this activity, subjects with severe ASD are to be identified using the cardiac condition labels of the general patient database.

7. When a patient is identified from the database, records and images pertaining to scans are extracted for data preparation and post-processing. The scanned images may be reloaded into the syngo Multi Modality Workplace system.
8. A section of each image is cropped from MR scans pertaining to all the phases at user-specified regions of interest. Due to the truncation in size, the image decreases in resolution to maintain a size with the same dimensions as the original one. Range of gray-scale intensity for all images is standardized. The images are converted into graphic files in BITMAP format. Alternatively, they may remain as DICOM format depending on the image format dictated by the medical imaging application.
9. The prepared MR images can be transferred out of the work station by means of a removable storage device or through a network cable. The user may now exit the syngo Multi Modality Workplace software.
10. The MR images are loaded into a DICOM decoder offline, and the images of the slice that dissects the left and right atria, showing the atrial septal defect (ASD), are selected for processing. This slice will demonstrate the abnormal cardiac flow through the ASD. The regions showing the right atria are truncated to the same dimensions for all images to prepare for flow visualization.
11. The images for pre- and post-septal occlusion are standardized at the same sizes (i.e. 156×192 pixels) in order to maintain consistency during computation and analysis.
12. The region of defect is examined and the extent of the ASD is recorded. The size of the defect can be measured and calibrated in S.I. units. The abnormal dilation of the right atrium is noted. Any other anomalies are observed and recorded.
13. The right chamber is selected for observation. The temporally varying flow pattern within the segmented chamber region of interest (ROI) is deduced heuristically.
14. The visual display rate is adjusted so that the registration of motion by human perception is optimal.
15. A manual sketch of the flow patterns is carried out. This may be assisted by fluid motion tracking output which can give an illustration of the general flow. The observation of ASD can be based on the flow fields and qualitative measures in the report. The patient is analyzed by comparing the vorticity level against a specified threshold to determine his cardiac condition. A strategy for cardiac management of the patient can be devised based

on the case study report. This is transferred electronically or in hard copy document to medical professionals for investigation.

5.3 Summary of Examination Pre- and Post-ASO by Intensity Images

Cardiac flow investigation procedures for cardiovascular defects using case studies of ASD patients (age ranges from 20 to 43 years at the time of scan) that are detailed in this section are performed and analysed from the structural and flow perspective. These procedures describe the process of performing MRI and decoding of MR images from DICOM format [94] to graphic files for post-processing of patient scans pre- and post-surgical intervention. All the procedural components, along with their critical specifications and execution are listed in point format for the user and with reference to a flow chart. In such examinations, MRI was conducted in accordance with guidelines defined by the hospital to achieve safe and reliable scanning. The scanning will be conducted after consent is obtained from patients when the imaging procedures had been conveyed. MR images based on the short axis (two-chamber) view of the heart showing the atria are presented as scan examples.

We present the qualitative flow observation that can be obtained using SSFP MRI data. The quantitative information on the atrial dimensions is presented. Note that for an effective comparison, we tried to ensure that the same imaging orientation and imaging slice are used. We investigate the flow patterns of blood in the right atrium by analysing the strength of vortices in vorticity flow maps. It is hypothesised that the vortices in a patient with ASD will be stronger and more coherent after septal occlusion. This is consistent with the previous study [9]. The flow maps superimposed onto MR images for pre- and post-ASD, and with the corresponding vorticity statistics are shown in Figure 13.

In terms of atrial dimensions, we have performed examinations of 26 ASD patients based on the procedures outlined in Section 5.2.2. We compute the ratio of right chamber area for pre-ASO to that for post-ASO for all the study subjects, and found that this population study has a dimensionless mean of 1.214 and a standard deviation of 0.0512. These results are shown in Figure 14. It is clear that ASO causes a reduction in the size of the right atrium. Furthermore, the flow patterns in the right atrium for 20 of the post-ASO cases are heuristically determined to have a stronger and more consistent rotation than they did before septal occlusion. For 6 of the case studies, we find difficulty in deducing the relative scale of rotation pre- and post-ASO due to poor imaging or lack of feature trackers that are able to stand out sufficiently for tracing the flow. A number of reasons contribute to the problem such as the limited number of features in a small field of view for some of the scans, occlusion of flow features due to void signals caused by the para-magnetic properties of the septal occluder, and selection of short axis planes that bisect the atrium such that its cross-sectional area is not at its maximum through the middle of

the chamber. In summary, based on Figure 11, we can conclude that ASO restores the chamber to a more normal size, and that there is a difference in their structural and flow characteristics pre- and post-ASO. This study shows that we are able to use MR fluid motion tracking to find a difference in flow patterns before and after surgical intervention.

6 Conclusion

With the technological advancement in medical imaging and cardiac flow analytical tools, there is a wealth of industries to research and improve the technology for the investigation of cardiac functions, and for the upgrading of medical diagnosis. This review has outlined the development of post-processing architecture for MR signal motion tracking in order to establish a new flow imaging technology. Towards the goal of the computer-aided MR fluid motion tracking is novel research on two parallel fronts. The first concerns harnessing of signal contrast to perform motion tracking. Multi-resolution optical flow is adapted to apply on gray-scale intensity MR images. On the second front, a flow characterisation framework is designed to develop flow and strain maps, and quantify flow behaviour in the heart chamber. The computerised MR fluid motion tracking framework is also demonstrated in case studies focusing on cardiac analysis of atrial septal defect patients. These represent just a myriad of potential non-invasive cardiac flow measurement and analysis applications.

Financial & Competing Interests Disclosure

Authors declare that there is Conflict of Interest or any financial involvement with any organisation or entity with a financial interest in or financial conflict with the subject matter or materials discussed in the manuscript. This includes employment, consultancies, honoraria, stock ownership or options, expert testimony, grants or patents received or pending, or royalties. No writing assistance was utilised in the production of this manuscript.

References

- [1]. Vasan, R.S., et al., *Congestive heart failure in subjects with normal versus reduced left ventricular ejection fraction*. Journal of the American College of Cardiology, 1999. 33: p. 1948-1955.
- [2]. Zile, M.R. and D.L. Brutsaert, *New Concepts in Diastolic Dysfunction and Diastolic Heart Failure: Part I*. Circulation, 2002. 105: p. 1387-1393.
- [3]. Hasegawa, H., et al., *Diastolic mitral annular velocity during the development of heart failure*. Journal of the American College of Cardiology, 2003. 41: p. 1590-1597.

- [4]. Gharib, M., et al., *A global index for heart failure based on optimal vortex formation in the left ventricle*. Proceedings of the National Academy of Sciences USA (PNAS), 2006. 103(16): p. 6305-6308.
- [5]. Carlhäll, C.J. and A. Bolger, *Passing strange: Flow in the failing ventricle*. Circulation: Heart Failure, 2010. 3: p. 326-331.
- [6]. Powell, A.J., et al., *Phase-Velocity Cine Magnetic Resonance Imaging Measurement of Pulsatile Blood Flow in Children and Young Adults: In Vitro and In Vivo Validation*. Pediatric Cardiology, 2000. 21: p. 104-110.
- [7]. Kilner, P.J., et al., *Asymmetric redirection of flow through the heart*. Nature Medicine, 2000. 404: p. 759-761.
- [8]. Markl, M., et al., *Time-Resolved 3D MR Velocity Mapping at 3T: Improved Navigator-Gated Assessment of Vascular Anatomy and Blood Flow*. Journal of Magnetic Resonance Imaging, 2007. 25: p. 824-831.
- [9]. Wong, K.K.L., et al., *Noninvasive Cardiac Flow Assessment Using High Speed Magnetic Resonance Fluid Motion Tracking*. PLoS ONE, 2009. 4(5): p. e5688.
- [10]. Wong, K.K.L., et al., *Theory and Validation of Magnetic Resonance Fluid Motion Estimation Using Intensity Flow Data*. PLoS ONE, 2009. 4(3): p. e4747.
- [11]. Wong, K.K.L., J.Y. Tu, and R.M. Kelso, *Vortical flow analysis*. Journal of Mechanics in Medicine and Biology, 2010. 10(2): p. 191–212.
- [12]. Hirsch, R., et al., *Diagnosis in adolescents and adults with congenital heart disease. Prospective assessment of individual and combined roles of magnetic resonance imaging and transthoracic echocardiography*. Circulation, 1994. 90: p. 2937-2951.
- [13]. Hoppe, U.C., et al., *Congenital heart disease in adults and adolescents: comparative value of transthoracic and transthoracic echocardiography and MR imaging*. Radiology, 1996. 199(3): p. 669-677.
- [14]. Abdel-Massih, T., et al., *Assessment of Atrial Septal Defect Size with 3D-Transthoracic Echocardiography: Comparison with Balloon Method*. Echocardiography, 2005. 22(2): p. 121-127.
- [15]. Kasliwal, R.R., et al., *Real-time three-dimensional transthoracic echocardiography*. Indian Heart Journal, 2005. 57(2): p. 128-137.
- [16]. Bartel, T., et al., *Single-plane Balloon Sizing of Atrial Septal Defects with Intracardiac Echocardiography: An Advantageous Alternative to Fluoroscopy*. Journal of the American Society of Echocardiography, 2008. 21(6): p. 737-740.
- [17]. Roldán, F.-J., et al., *Three-dimensional transthoracic echocardiography of the atrial septal defects*. Cardiovascular Ultrasound, 2008. 6(1): p. 38.
- [18]. Piatkowski, R., P. Scislo, and J. Kochanowski, *Transthoracic real-time three-dimensional echocardiography in assessing large multiperforated atrial septal aneurysm*. European Heart Journal, 2009(doi:10.1093/eurheartj/ehp019).
- [19]. Skolnick, A., E. Vavas, and I. Kronzon, *Optimization of ASD Assessment using Real Time Three-Dimensional Transthoracic Echocardiography*. Echocardiography, 2009. 26(2): p. 233-235.
- [20]. Fujio, K., et al., *MRI apparatus for receiving nuclear-magnetic resonance signals of a living body*. Magnetic Resonance Imaging, 1995. 13(7): p. XII-XII(1).
- [21]. Fujio, K., et al., *MRI apparatus for receiving nuclear-magnetic resonance signals of a living body*. 1995: United States Patent Application, US Patent 5427103.
- [22]. Hong, G.-R., et al., *Characterization and quantification of vortex flow in the human left ventricle by contrast echocardiography using vector particle image velocimetry*. J Am Coll Cardiol Img, 2008. 1: p. 705-717.

- [23]. Kheradvar, A., et al., *Echocardiographic particle image velocimetry: a novel technique for quantification of left ventricular blood vorticity pattern*. J Am Soc Echocardiogr, 2010. 23(1): p. 86-94.
- [24]. Phillips, *Philips Medical Systems Clinical Education, Basic principles of MR imaging*,. 1984.
- [25]. Worthley, S.G., *Magnetic Resonance Imaging of Atherosclerotic Plaque*. 2001, University of Adelaide.
- [26]. Worthley, S.G. and Z.A. Fayad, *Utility of cardiovascular magnetic resonance imaging*. Heart, Lung and Circulation, 2002. 11: p. 63.
- [27]. Bloomer, T.N., et al., *Cine MRI using steady state free precession in the radial long axis orientation is a fast accurate method for obtaining volumetric data of the left ventricle*. Journal of Magnetic Resonance Imaging, 2001. 14(6): p. 685-692.
- [28]. Markl, M. and N.J. Pelc, *On flow effects in balanced steady-state free precession imaging: pictorial description, parameter dependence, and clinical implications*. Journal of Magnetic Resonance Imaging, 2004. 20(4): p. 697-705.
- [29]. Li, W., et al., *Dark flow artifacts with steady-state free precession cine MR technique: Causes and implications for cardiac MR imaging*. Radiology, 2004. 230: p. 569-575.
- [30]. Plein, S., et al., *Steady-state free precession magnetic resonance imaging of the heart: Comparison with segmented k-space gradient-echo imaging*. Journal of Magnetic Resonance Imaging, 2001. 14(3): p. 230-236.
- [31]. Gleeson, T.G., et al., *Steady-state free-precession (SSFP) cine MRI in distinguishing normal and bicuspid aortic valves*. Journal of Magnetic Resonance Imaging, 2008. 28: p. 873-878.
- [32]. Chen, Q., et al., *A Breath-hold Three Dimensional True FISP Sequence for Abdominal MRI*. Proceedings of the International Society for Magnetic Resonance in Medicine, 2001. 9: p. 232.
- [33]. Herborn, C.U., et al., *MRI of the liver: Can true FISP replace HASTE?* Journal of Magnetic Resonance Imaging, 2003. 17(2): p. 190-196.
- [34]. Carr, J.C., et al., *Cine MR Angiography of the Heart with Segmented True Fast Imaging with Steady-State Precession*. Radiology, 2001. 219: p. 828-834.
- [35]. Fuchsa, F., G. Laubb, and K. Othomoc, *TrueFISP—technical considerations and cardiovascular applications*. European Journal of Radiology, 2003. 46(1): p. 28.
- [36]. Kellman, P., et al., *Cardiac First-pass Perfusion MRI using 3D trueFISP Parallel Imaging using TSENSE*. Proceedings of the International Society for Magnetic Resonance in Medicine, 2004. 11: p. 310.
- [37]. Kuethe, D.O., *Measuring distributions of diffusivity in turbulent fluids with magnetic-resonance imaging*. Physical Review A, 1989. 40: p. 4542-4551.
- [38]. Globits, S. and C.B. Higgins, *Assessment of valvular heart disease by magnetic resonance imaging*. American Heart Journal, 1995. 129(2): p. 369-81.
- [39]. Lawson, M.A., *Cardiovascular imaging in the new millennium*. Proceedings of the Baylor University Medical Center (BUMC), 1999. 12: p. 115-120.
- [40]. Horn, B.K.P. and B.G. Schunck, *Determining Optical Flow*. Artificial Intelligence, 1981. 17: p. 185-203.
- [41]. Barron, J.L., D.J. Fleet, and S.S. Beauchemin, *Performance of optical flow techniques*. International Journal of Computer Vision, 1994. 12(1): p. 43-77.
- [42]. Guiterrez, M.A., et al., *Myocardial Motion Estimation in Gated-MRI Using Optical Flow Refined with Scale-Space*. Computers on Cardiology, 1997. 24: p. 153-156.
- [43]. Merrifield, R., et al., *Dual Contrast TrueFISP Imaging for Left Ventricular Segmentation*. Magnetic Resonance in Medicine, 2001. 46(5): p. 939-945.
- [44]. Higgins, C.B., et al., *Evaluation of myocardial function and perfusion in ischemic heart disease*. Magnetic Resonance Materials in Physics, Biology and Medicine, 1994. 2(3): p. 177-184.

- [45]. Manna, A.L., N. Sutaria, and S.K. Prasad, *MRI in Ischemic heart disease: From coronaries to myocardium*. Indian Journal of Radiology and Imaging, 2007. 17(2): p. 98-108.
- [46]. Nienaber, C.A., et al., *The diagnosis of thoracic aortic dissection by noninvasive imaging procedures*. New England Journal of Medicine, 1993. 328(22): p. 1637.
- [47]. Deutsch, H.J., et al., *Chronic aortic dissection: comparison of MR imaging and transesophageal echocardiography*. Radiology, 1994. 192: p. 645-650.
- [48]. Laissy, J.P., et al., *Thoracic aortic dissection: diagnosis with transesophageal echocardiography versus MR imaging*. Radiology, 1995. 194: p. 331-336.
- [49]. Moore, E.H., et al., *MRI of chronic posttraumatic false aneurysms of the thoracic aorta*. American Journal of Roentgenology, 1984. 143(6): p. 1195-1196.
- [50]. Dinsmore, R.E., et al., *Magnetic resonance imaging of thoracic aortic aneurysms: comparison with other imaging methods*. American Journal of Roentgenology, 1986. 146(2): p. 309-314.
- [51]. Stauder, N.I., et al., *MRI diagnosis of a previously undiagnosed large trabecular ventricular septal defect in an adult after multiple catheterizations and angiocardiograms*. British Journal of Radiology, 2001. 74: p. 280-282.
- [52]. Puvaneswary, M., T. Singham, and B. Bastian, *Atrial septal aneurysm: MRI and echocardiography correlation*. Australasian Radiology, 2003. 47(4): p. 468-471.
- [53]. Webb, G. and M.A. Gatzoulis, *Atrial septal defects in the adult - Recent progress and overview*. Circulation, 2006. 114: p. 1645-1653.
- [54]. Beerbaum, P., et al., *Atypical atrial septal defects in children: noninvasive evaluation by cardiac MRI*. Pediatric Radiology, 2008. 38(11): p. 1188-1194.
- [55]. Deshpande, V.S., et al., *3D magnetization-prepared true-FISP: a new technique for imaging coronary arteries*. Magn Reson Med, 2001. 46: p. 494-502.
- [56]. Hundley, W.G., et al., *Assessment of coronary arterial flow and flow reserve in humans with magnetic resonance imaging*. Circulation, 1996. 93: p. 1502-1508.
- [57]. Hundley, W.G., et al., *Assessment of coronary arterial restenosis with phase-contrast magnetic resonance imaging measurements of coronary flow reserve*. Circulation, 2000. 101: p. 2375-2381.
- [58]. Sakuma, H. and C.B. Higgins, *Magnetic resonance measurement of coronary blood flow*. Acta Paediatr Suppl, 2004. 93: p. 80-85.
- [59]. English, P.T. and C. Moore, *MRI for Radiographers*. 1995: Springer-Verlag London, Great Britain.
- [60]. Wong, K.K.L., et al., *Medical Imaging And Processing Methods For Cardiac Flow Reconstruction*. Journal of Mechanics in Medicine and Biology, 2009. 9(1): p. 1-20.
- [61]. Palaniappan, K., et al., *Structure and Semi-fluid motion analysis of stereoscopic satellite images for cloud tracking*. Proceedings of the 5th International Conference on Computer Vision, 1995: p. 659-665.
- [62]. Giachetti, A. and V. Torre, *Optical Flow and Deformable Objects*. Proceedings of the 5th International Conference on Computer Vision, 1995: p. 706.
- [63]. Giachetti, A. and V. Torre, *The use of optical flow for the analysis of non-rigid motions*. International Journal of Computer Vision archive, 1996. 18(3): p. 255-279.
- [64]. Gladden, L.F., *Nuclear magnetic resonance in chemical engineering: principles and applications*. Chemical Engineering Science, 1994. 49(20): p. 3339-3408.
- [65]. Gladden, L.F. and P. Alexander, *Applications of nuclear magnetic resonance imaging in process engineering*. Measurement Science and Technology, 1996. 7: p. 423-435.
- [66]. Akpa, B.S., et al., *Enhanced (13)C PFG NMR for the study of hydrodynamic dispersion in porous media*. Journal of Magnetic Resonance Imaging, 2007. 18(1): p. 160-165.
- [67]. Akpa, B.S., et al., *Study of miscible and immiscible flows in a microchannel using magnetic resonance imaging*. Analytical Chemistry, 2007. 79(16): p. 6128-6134.

- [68]. Graf von der Schulenburg, D.A., et al., *Non-invasive mass transfer measurements in complex biofilm-coated structures*. Biotechnology and Bioengineering, 2008. 101(3): p. 602-608.
- [69]. Rehwald, W.G., et al., *Noninvasive cineangiography by magnetic resonance global coherent free precession*. Nature Medicine, 2004. 10: p. 545-549.
- [70]. Klem, I., et al., *Noninvasive assessment of blood flow based on magnetic resonance global coherent free precession*. Circulation, 2005. 111: p. 1033-1039.
- [71]. Alsop, D., *Arterial spin labeling with pulsed radio frequency sequences*. United States Patent Application, \rm US 2007/0132452 A1, 2007.
- [72]. Horowitz, A.L., *MRI Physics for Radiologists - A Visual Approach, 3rd edition*. 1994: Springer-Verlag, New York, USA.
- [73]. Markl, M., et al., *Time-resolved three-dimensional phase-contrast MRI*. Journal of Magnetic Resonance Imaging, 2003. 17: p. 499-506.
- [74]. Yu, Q., X. Kong, and D. Liu, *Differential diagnosis of arachnoid cyst from subarachnoid space enlargement by phase-contrast cine MRI*. Chinese Medical Journal, 2003. 116(1): p. 116-120.
- [75]. Duncan, R.F., K.S.L. Teo, and S.G. Worthley, *Cardiac magnetic resonance documentation of a double atrial septal defect before and after percutaneous closure with an Amplatzer septal occluder*. International Journal of Cardiology, 2008. 130(1): p. e42-e43.
- [76]. McMahon, C.J., et al., *Natural history of growth of secundum atrial septal defects and implications for transcatheter closure*. Heart, 2002. 87(3): p. 256-259.
- [77]. Linguraru, M.G., et al., *Fast block flow tracking of atrial septal defects in 4D echocardiography*. Medical Image Analysis, 2008. 12(4): p. 397-412.
- [78]. Sprecher, D.L., et al., *In vitro color flow, pulsed and continuous wave Doppler ultrasound masking of flow by prosthetic valves*. American College of Cardiology, 1987. 9: p. 1306-1310.
- [79]. Tamai, J., et al., *Improvement in mitral flow dynamics during exercise after percutaneous transvenous mitral commissurotomy. Noninvasive evaluation using continuous wave Doppler technique*. Circulation, 1990. 81: p. 46-51.
- [80]. Walker, A., et al., *Accuracy of spectral Doppler flow and tissue velocity measurements in ultrasound systems*. Ultrasound in Medicine & Biology, 2004. 30(1): p. 127-132.
- [81]. Park, M., J.S. Jin, and S. Luo, *A Novel Approach for Enhancing the Visual Perception of Ribs in Chest Radiography*. Proceedings of the IEEE/ICME International Conference on Complex Medical Engineering (ICME 2007), Beijing, China, 2007.
- [82]. Egeblad, H., et al., *Non-invasive diagnosis in clinically suspected atrial septal defect of secundum or sinus venosus type. Value of combining chest x-ray, phonocardiography, and M-mode echocardiography*. British Heart Journal, 1980. 44(3): p. 317-321.
- [83]. Wolbarst, A.B., *Looking Within How X-ray, CT, MRI, Ultrasound, and Other Medical Images are Created, and How They Help Physicians Save Lives*. 1999: University of California Press, USA.
- [84]. Wong, K.K.L., et al., *Cardiac Flow Analysis Applied to Phase Contrast Magnetic Resonance Imaging of the Heart*. Annals of Biomedical Engineering, 2009. 37(8): p. 1495-1515.
- [85]. Wong, K.K.L., et al., *Cardiac Flow Component Analysis*. Medical Engineering & Physics, 2010. 32(2): p. 174-188.
- [86]. Fyrenius, A., et al., *Three dimensional flow in the human left atrium*. Heart, 2001. 86: p. 448-455.
- [87]. Pierrakos, O. and P.P. Vlachos, *The effect of vortex formation on left ventricular filling and mitral valve efficiency*. Journal of Biomechanical Engineering-Transactions of ASME, 2006. 128(4): p. 527-539.
- [88]. Yang, G.Z., et al., *Vortical flow feature recognition: A topological study of in-vivo flow patterns using MR velocity mapping*. Journal of Computer Assisted Tomography, 1998. 22: p. 577-586.

- [89]. Cross, R.R., et al., *Three-Dimensional Imaging of Atrial Septal Occlusion Device*. *Pediatric Cardiology*, 2001. 22(5): p. 427-428.
- [90]. Kim, M.S., A.J. Klein, and J.D. Carroll, *Transcatheter Closure of Intracardiac Defects in Adults*. *Journal of Interventional Cardiology*, 2007. 20(6): p. 524-545.
- [91]. Balzer, J., H. Kühl, and A. Franke, *Real-time three-dimensional transoesophageal echocardiography for guidance of atrial septal defect closures*. *European Heart Journal*, 2008. 29(18): p. 2226.
- [92]. Webb, W.R. and C.B. Higgins, *Thoracic Imaging: Pulmonary and Cardiovascular Radiology*. 2004: Lippincott Williams & Wilkins.
- [93]. Teo, K.S.L., et al., *Percutaneous closure of atrial septal defects leads to normalisation of atrial and ventricular volumes*. *Journal of Magnetic Resonance Imaging*, 2008. 10(1): p. 55.
- [94]. Parisot, C., *The DICOM standard: A breakthrough for digital information exchange in cardiology*. *International Journal of Cardiac Imaging*, 1995. 11(3): p. 171-177.

List of Figure Legends

Figure 1: **Feature of precessing blood proton spins.** Hydrogen-based molecules of blood maintain coherent spin phases when assuming a static fluid state as displayed by A, but are distributed chaotically in turbulent fluid and this disrupts the alignment of proton spins from their order as shown in B. Due to the incoherent or random precession of spins, the net magnetisation is weak and gives a low MR signal intensity. Therefore regions of blood at different levels of turbulence appear with contrasting pixel intensities in the cardiac MR image. The groups of incoherently precessing proton spins move along with the global blood flow within the cardiac chamber.

Figure 2: **Cardiac magnetic resonance imaging based on different configurations.** Cardiac magnetic resonance scans are based on different configurations depending on the cardiac examination such as the short axis view in subfigure A and long axis view in subfigure B. The abbreviations for the heart structures and scan configurations are: left atrium (LA), left ventricle (LV), right atrium (RA), right ventricle (RV), anterior septum (AS), inferior septum (IS), inferior (Inf), lateral (Lat), and anterior (Ant), left ventricular outflow tract view (LVOT), horizontal long axis (HLA). An appropriate scan view and multiple slices in a scan orientation enable us to examine different portions of the heart effectively.

Figure 3: **Cardiac magnetic resonance image views.** Display of cardiac magnetic resonance images is based on the short axis and also on the long axis (with 2-chamber, 3-chamber and 4-chamber views). Each configuration is selected to show the relevant chambers and cardiovascular structures with clarity. Different orientations display the chamber of interest at various positions and bisections. Is this an original image or adapted from some reference? I have seen similar image before about the MR imaging principle.

Figure 4: **Motion estimation of in-plane MR-signals.** Based on schematic display of a right atrial flow, the ensembles of asynchronous proton spins that show up as contrasting signal intensity on the cine-magnetic resonance images are represented by grey patches of varying intensity. Based on motion estimation, motion pertaining to the blood flow images of arbitrary $(n-1)$, n and $(n+1)$ phases in a cardiac cycle of N phases can be predicted.

Figure 5: **Cardiac diagnostic system.** System integration of sub-components results in the cardiac diagnostic that can facilitate examination of cardiac patients. From the flow perspective, we are able to detect the difference in patterns and vorticity quantifications for examination of cardiovascular defects.

Figure 6: **Circulation in a heart with atrial septal defect.** Cardiac defect such as atrial septal defect can affect the efficiency of circulation of oxygenated blood through the human body. (A) In this diagram, we examine the leak of oxygenated blood from the left atrium into the right. Therefore, a patient with the septal defect may not have the same health fitness standard in comparison with someone who has a normal healthy heart. (B) Here, IVC, SVC and TV denotes inferior vena cava, superior vena cava and tricuspid valve respectively.

Figure 7: **Schematic illustration of atrial septal occlusion.** Surgical intervention such as atrial septal occlusion (ASO) can help to seal the leakage from left atrium (LA) to right atrium (RA). This schematic diagram, illustrates how the septal occluder is inserted via a catheter using minimally invasive surgical intervention. The occluder is a circular mesh mechanism that is secured in a canister of the catheter, and upon reaching the site of defect, can be released to open up like an umbrella that locks itself onto the septum, and becoming part of it. The double folds of this mesh acts as a self-centering device that stabilise the position of occlusion and ensure an optimal ASD closure. Over time, the cardiac tissue grows into the occluder mesh and seals up the defect. This prosthetic device stays in the patient permanently.

Figure 8: **Myocardial discontinuity in a heart with atrial septal defect.** The MRI imaging of a heart based on short axis orientation is able to demonstrate the physical discontinuity of the myocardium that separates the left atrium (LA) and right atrium (RA) within the heart of an ASD patient. Medical examination based on this method can determine the location, size and extent of the defect. This can effectively diagnose the medical condition and plan for surgical preparation.

Figure 9: **Flow chart for guiding investigation of cardiac abnormalities.** A flow chart for MRI preparation and processing pertaining to those of cardiac patients is presented for systematic retrieval of cases and analysis of flow behaviour in heart. The breakdown of the cardiac investigation into stages allows a clear understanding of the rationale behind each activity and provides clear instruction for running them.

Figure 10: **Vorticity visualization of segmented right atrium pre- and post-ASD.** Vorticity flow maps (based on three slices) at a selected phase of cardiac cycle are superimposed onto cardiac MR image. The color representation of the flow map can be referenced against scales (in metric units of per second) to gauge the vorticity value. The characteristic for the vorticity map can be presented in frequency graphs as an indication of vorticity magnitudes represented by intensity pixels in the flow grid. The graphs show that the vorticity is amplified after septal occlusion. Statistical parameters include the mean $\overline{\omega}$, and standard deviation σ that are with respect to the histogram mean μ and median m . Both the means and standard deviation for pre-ASO are higher for post-ASO vorticity flow maps.

Figure 11: **Graph of chamber size ratios pre- and post-ASO.** The histogram of chamber size ratios for pre-ASO to post-ASO is presented for 26 patients. Of these 26 studies, 6 of them are deemed to be difficult cases for heuristic determination of relative flow either for the pre-ASO or the post-ASO cases. This results from the limitations in obtaining good contrast of asynchronous proton spins during imaging, and resolution of the scan image. Nevertheless, the results can demonstrate the difference between the two cases.

List of Figures

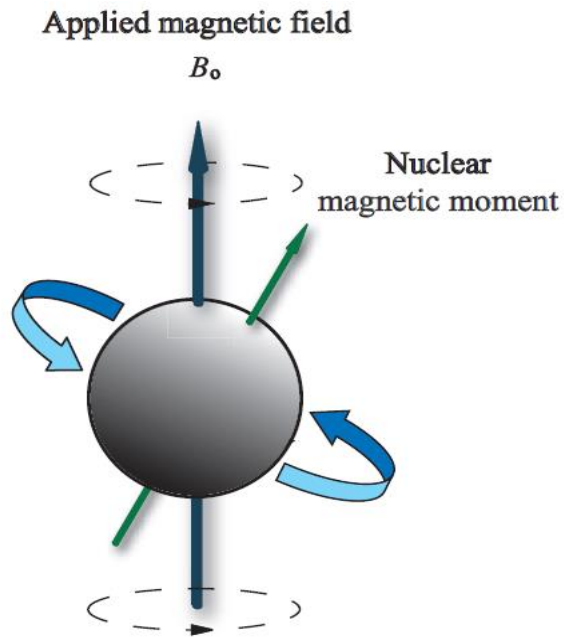


Figure 1

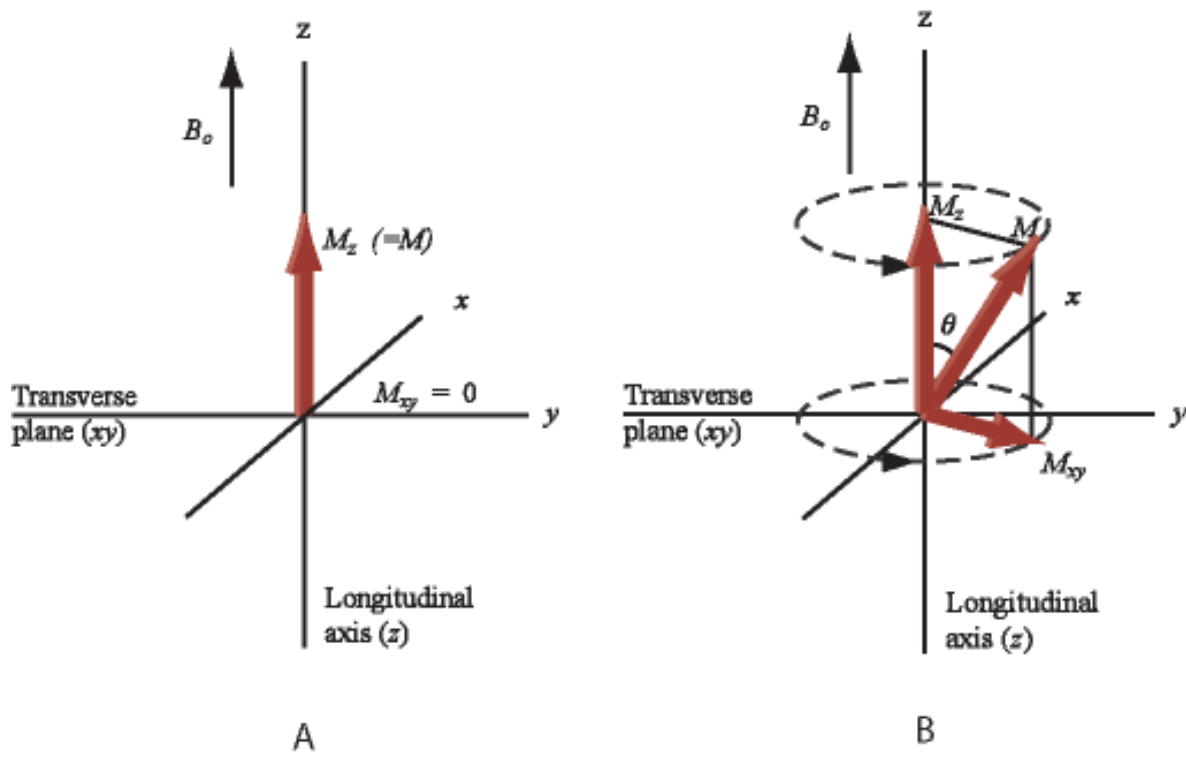


Figure 2

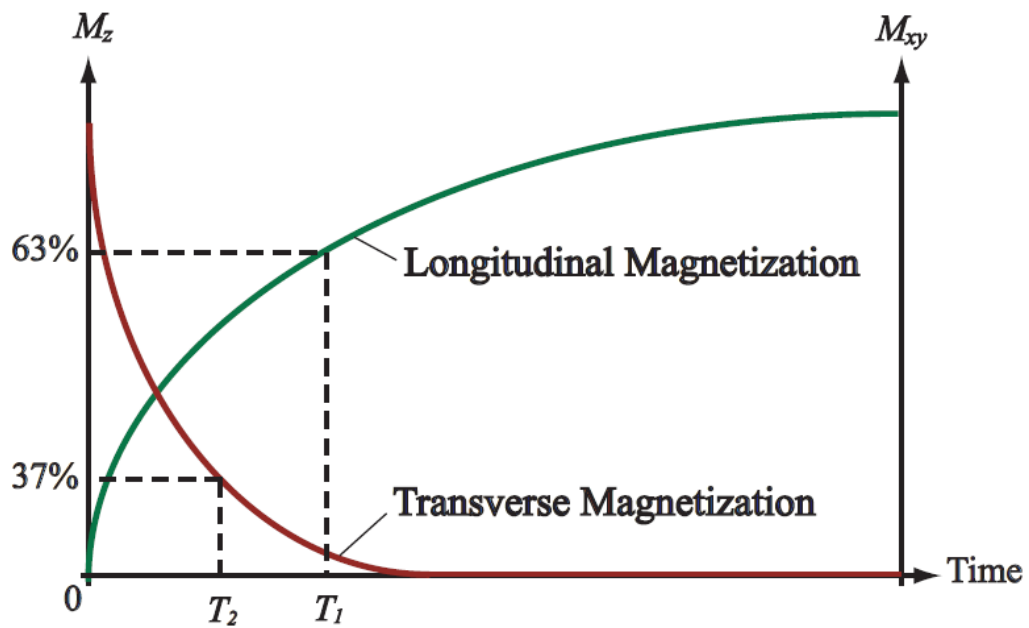


Figure 3

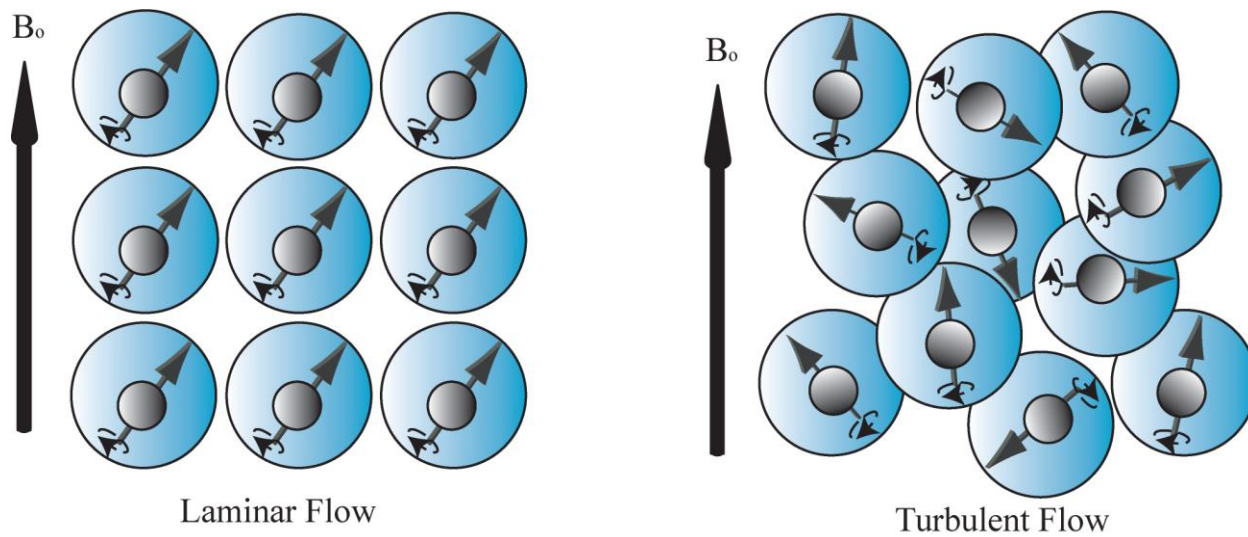


Figure 4

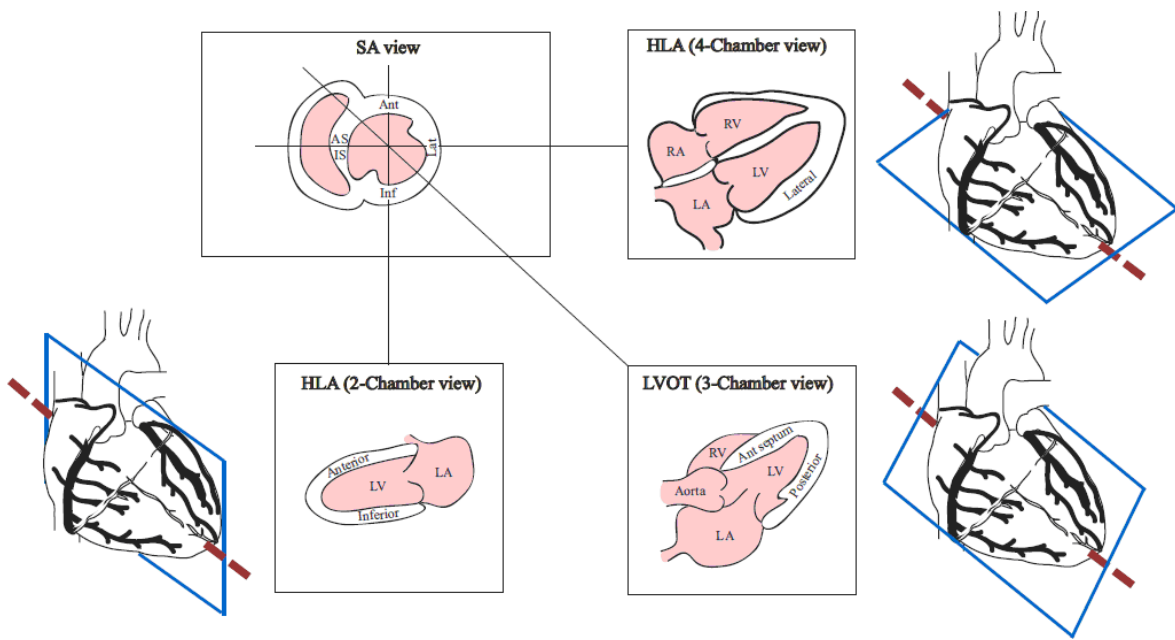


Figure 5

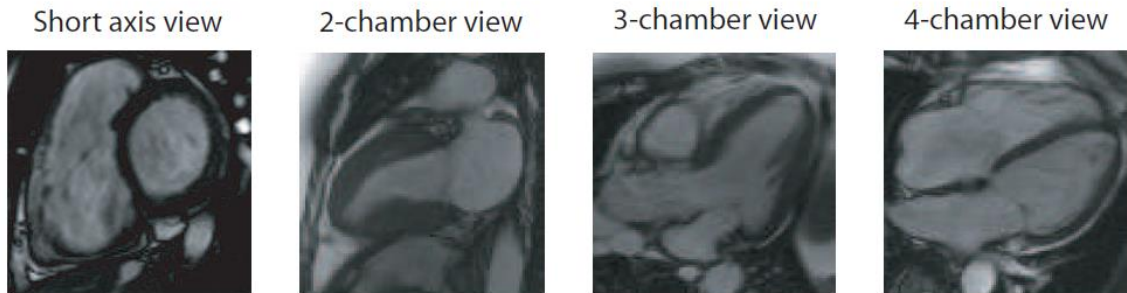


Figure 6

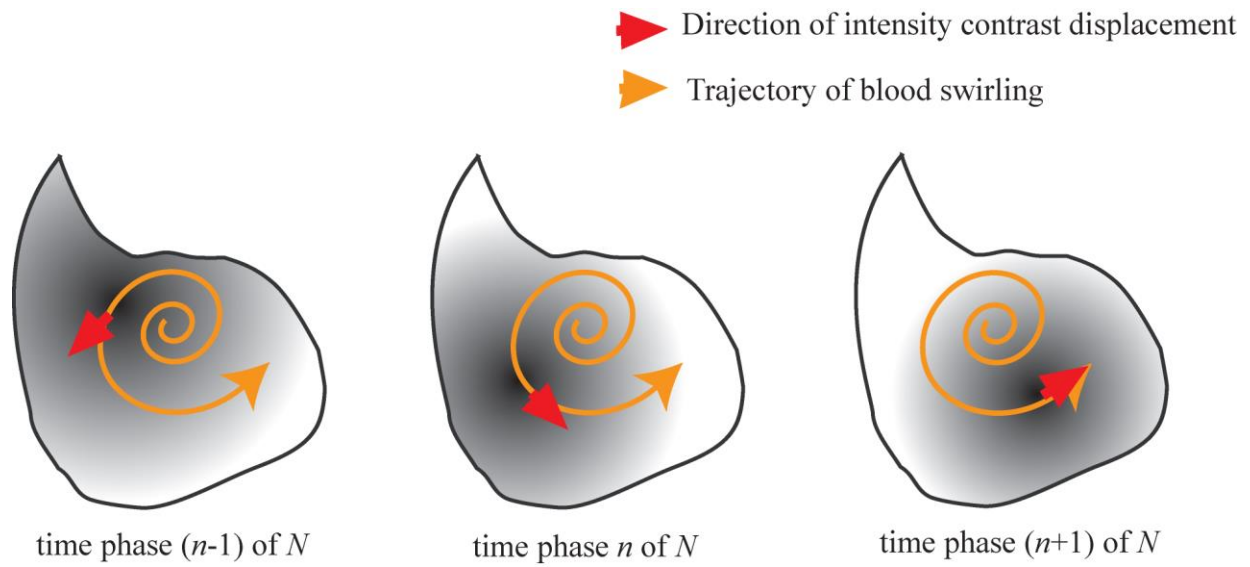


Figure 7

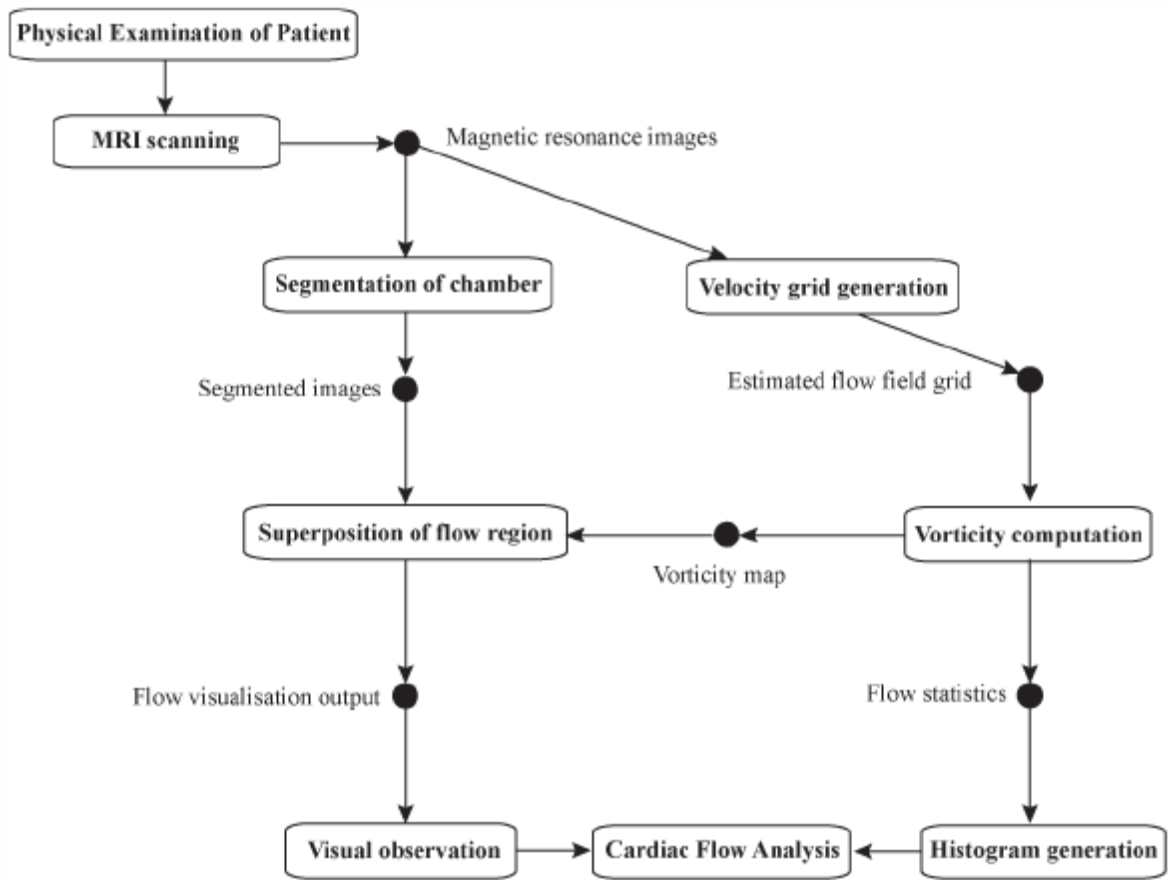
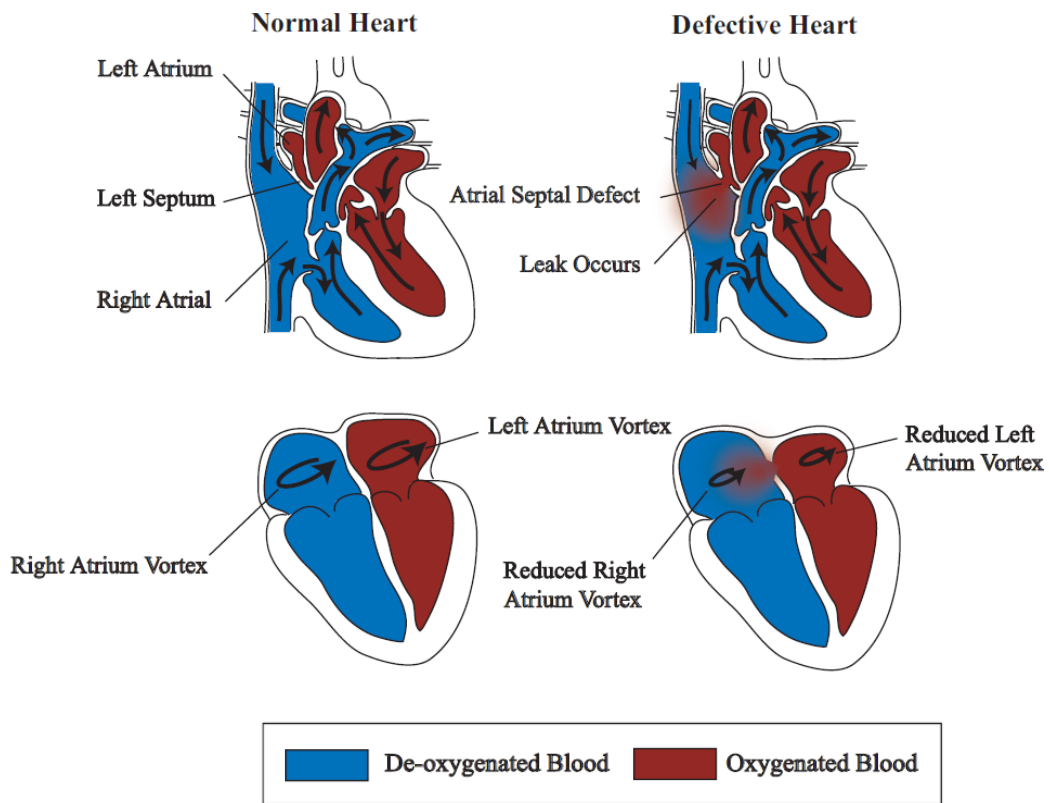
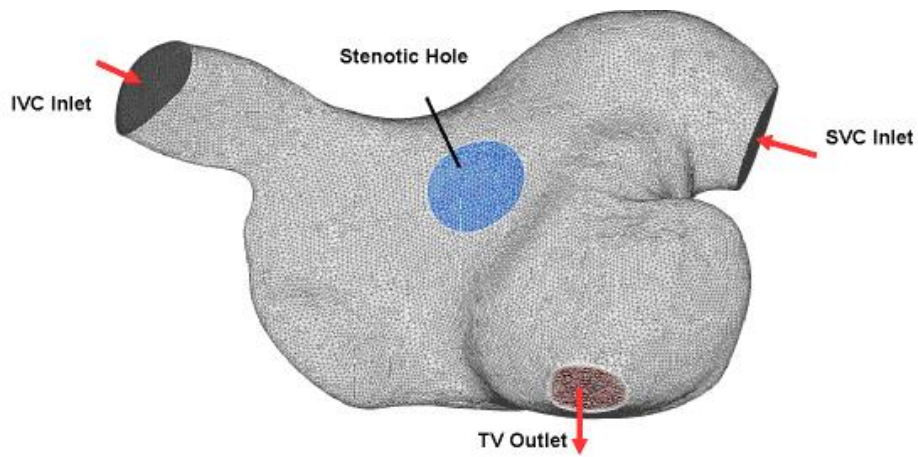


Figure 8



A



B

Figure 9

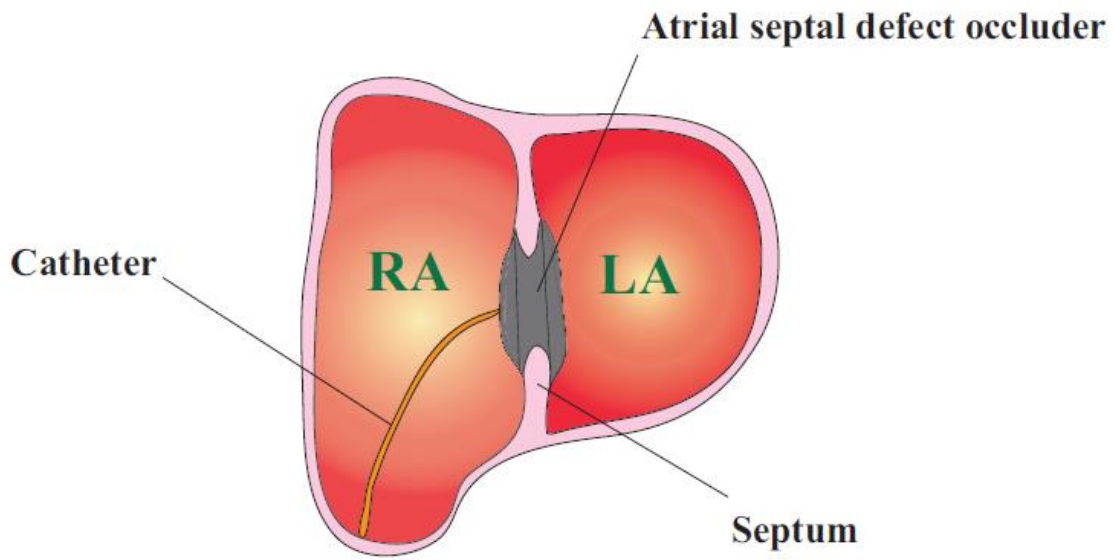


Figure 10

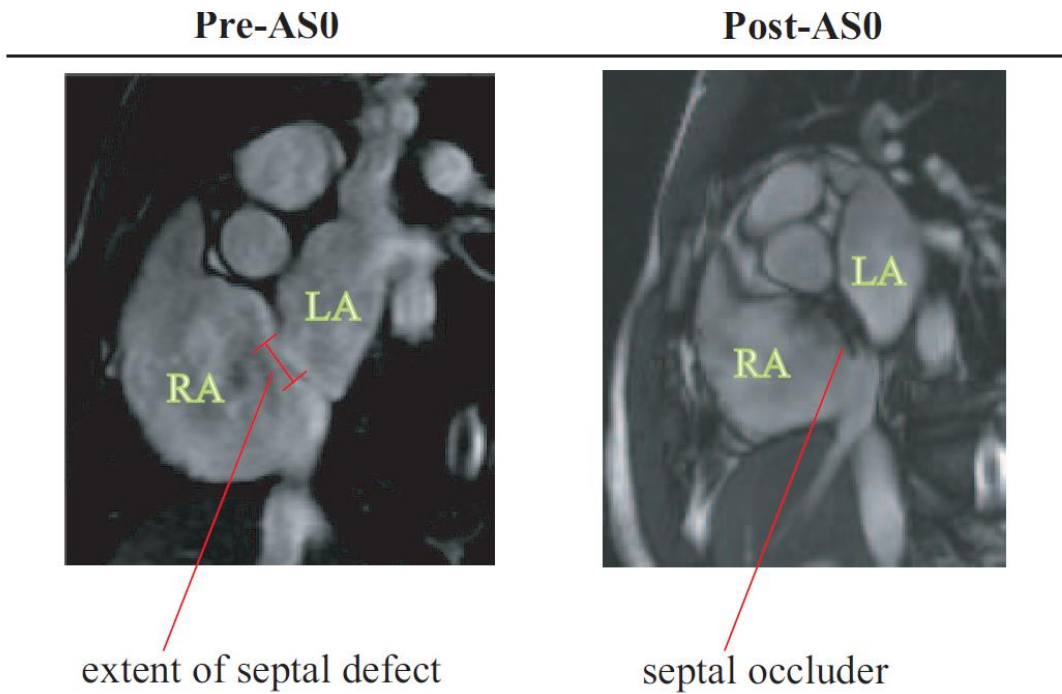


Figure 11

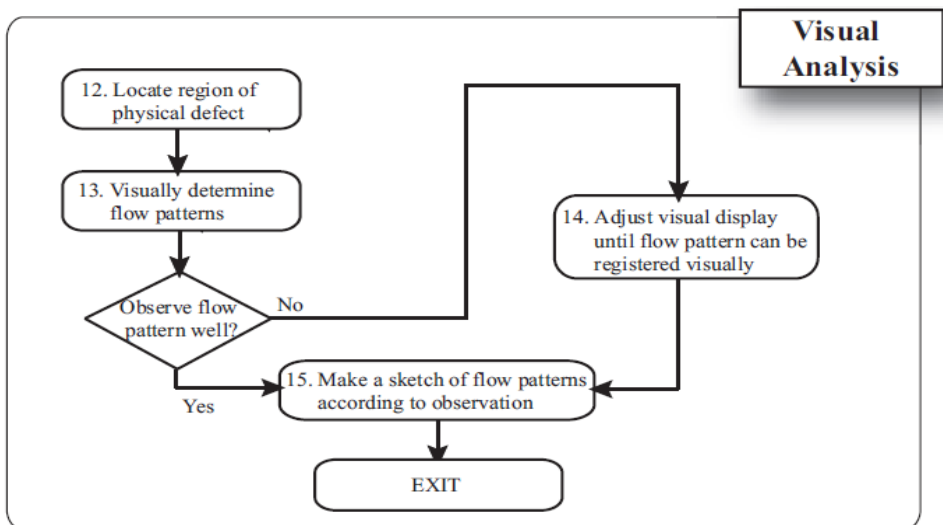
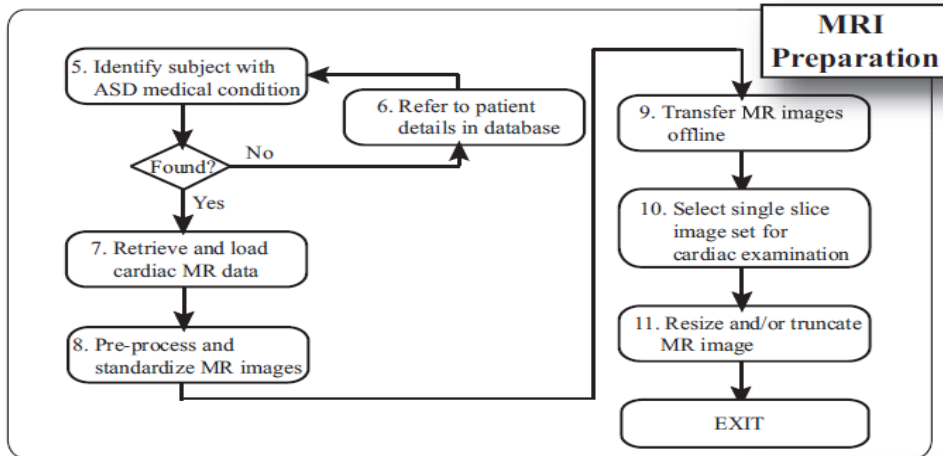
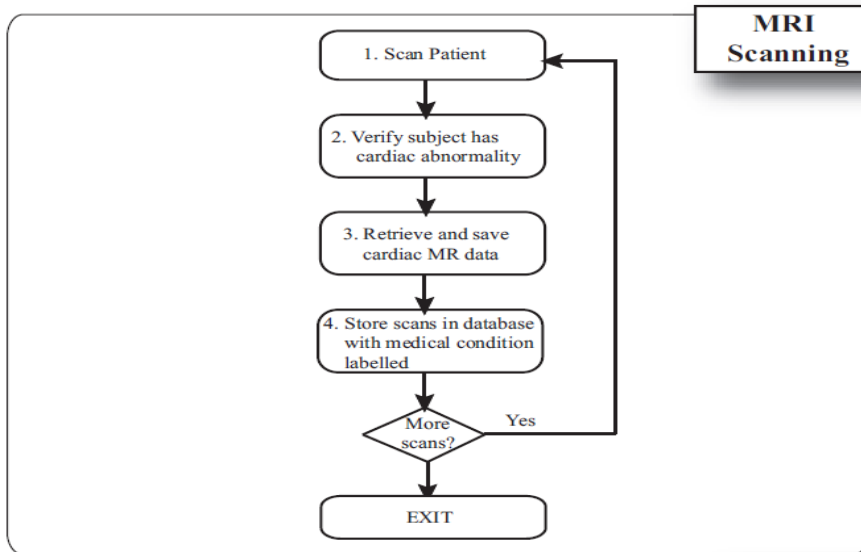
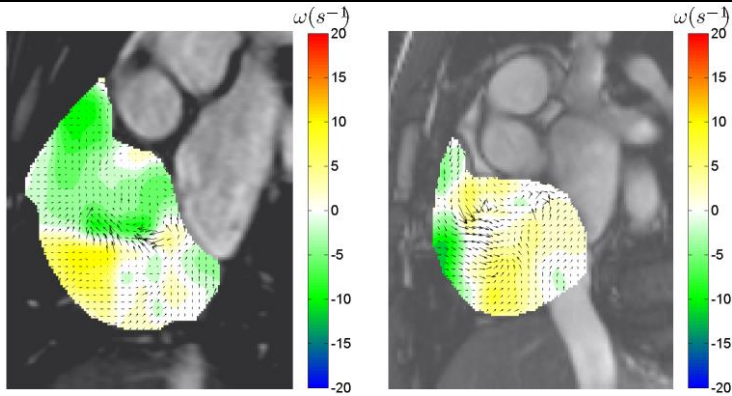


Figure 12

PRE-ASO

POST-ASO

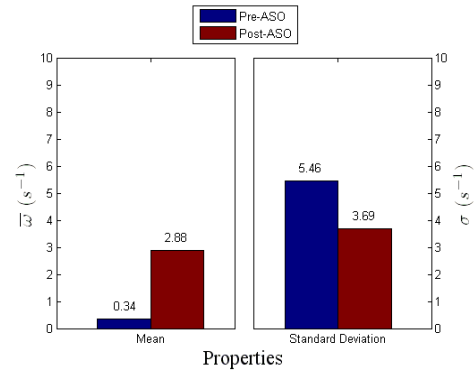
VORTICITY COMPARISON



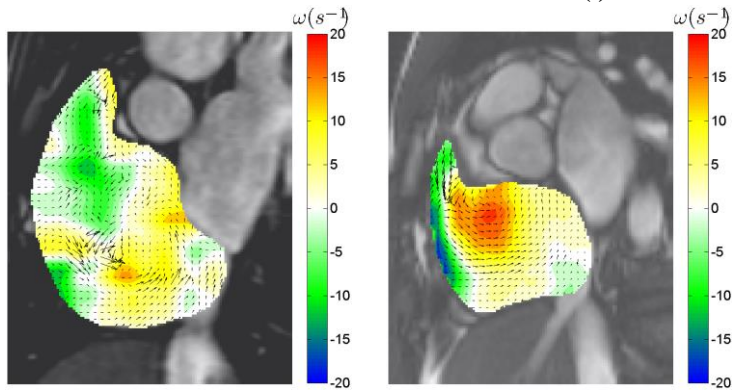
Pre-ASO:
$$\begin{bmatrix} \bar{\omega} \\ \bar{\sigma} \end{bmatrix}_\mu = \begin{bmatrix} 0.78 \\ 4.18 \end{bmatrix} s^{-1}$$

Post-ASO:
$$\begin{bmatrix} \bar{\omega} \\ \bar{\sigma} \end{bmatrix}_\mu = \begin{bmatrix} 4.58 \\ 5.20 \end{bmatrix} s^{-1}$$

(i) Slice 1



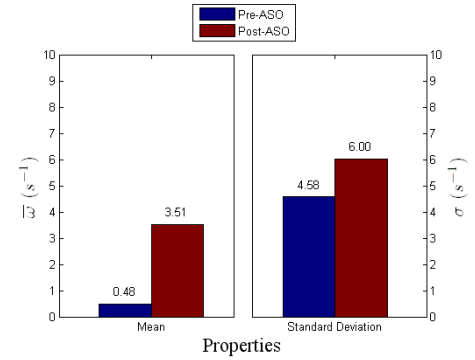
Ratio of $\bar{\omega}$ = 5.87
Ratio of $\bar{\sigma}$ = 1.24



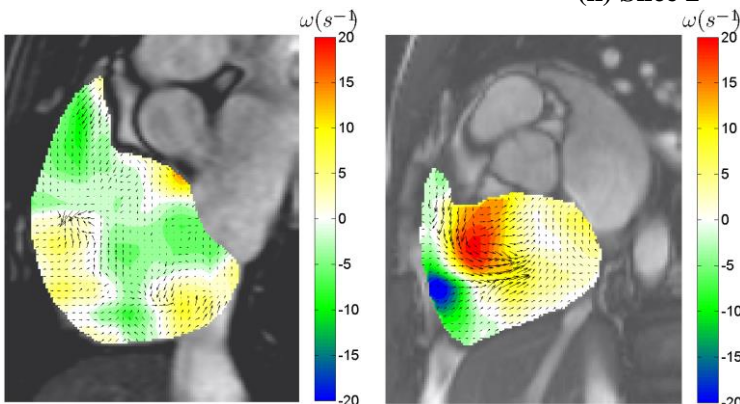
Pre-ASO:
$$\begin{bmatrix} \bar{\omega} \\ \bar{\sigma} \end{bmatrix}_\mu = \begin{bmatrix} 1.38 \\ 4.14 \end{bmatrix} s^{-1}$$

Post-ASO:
$$\begin{bmatrix} \bar{\omega} \\ \bar{\sigma} \end{bmatrix}_\mu = \begin{bmatrix} 5.17 \\ 6.39 \end{bmatrix} s^{-1}$$

(ii) Slice 2



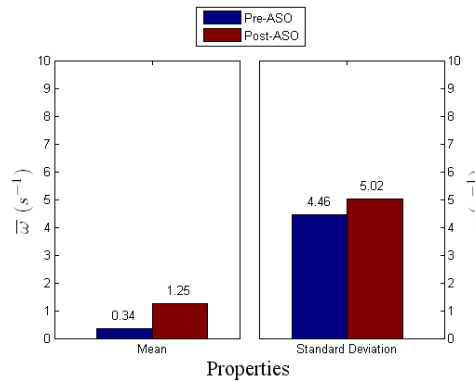
Ratio of $\bar{\omega}$ = 3.75
Ratio of $\bar{\sigma}$ = 1.53



Pre-ASO:
$$\begin{bmatrix} \bar{\omega} \\ \bar{\sigma} \end{bmatrix}_\mu = \begin{bmatrix} 0.61 \\ 3.36 \end{bmatrix} s^{-1}$$

Post-ASO:
$$\begin{bmatrix} \bar{\omega} \\ \bar{\sigma} \end{bmatrix}_\mu = \begin{bmatrix} 2.50 \\ 5.86 \end{bmatrix} s^{-1}$$

(iii) Slice 3
Figure 13



Ratio of $\bar{\omega}$ = 4.10
Ratio of $\bar{\sigma}$ = 1.74

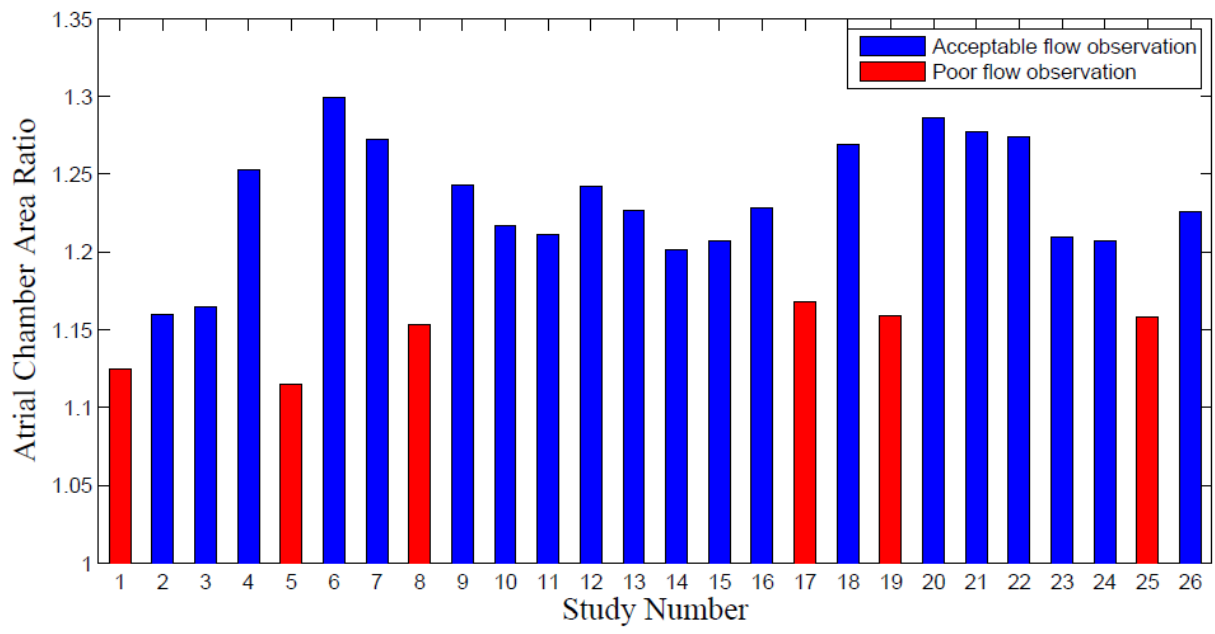


Figure 14